HEAT TRANSFER ENHANCEMENT IN HEAT EXCHANGERS USING COMPOUND ENHANCEMENT

By

Mouhsine Benmbarek

Bachelor of Science - Aerospace Engineering
International University of Rabat
2018

Master of Science - Mechanical Engineering
Mississippi State University
2019

A dissertation submitted in partial fulfillment
of the requirements for the

Doctor of Philosophy – Mechanical Engineering

Department of Mechanical Engineering
Howard R. Hughes College of Engineering
The Graduate College

University of Nevada, Las Vegas
May 2024

UNLV | GRADUATE COLLEGE

Dissertation Approval

The Graduate College
The University of Nevada, Las Vegas

November 29, 2023

This dissertation prepared by

Mouhsine Benmbarek

entitled

Heat Transfer Enhancement in Heat Exchangers Using Compound Enhancement

is approved in partial fulfillment of the requirements for the degree of

Doctor of Philosophy – Mechanical Engineering
Department of Mechanical Engineering

Samir Moujaes, Ph.D.
Examination Committee Chair

Alexander Barzilov, Ph.D.
Examination Committee Member

Mohamed Trabia, Ph.D.
Examination Committee Member

Moses Karakouzian, Ph.D.
Graduate College Faculty Representative

Alyssa Crittenden, Ph.D.
Vice Provost for Graduate Education & Dean of the Graduate College

ABSTRACT

This research will try to investigate the enhancement of heat transfer in a heat exchanger that is made of a corrugated tube that has a twisted plate inserted in it, the corrugation, and twisted plate are expected to increase the amount of heat transfer since the plate is acting as a connection between the center of the flow and the edges of the tube. The turbulence will cause an increase in pressure drop along the channel length, so the investigation will try to find the best compromise between the gain in heat transfer and loss of hydraulic energy by using well-established metrics. A positive heat transfer gain has been achieved if that metric indicates a value equal to or greater than 1. This CFD research will be compared with the experimental results by Zimparov (2012). After validating the CFD results it is proposed to investigate a new insert geometry to further improve the efficiency of the said heat exchanger.

The computational fluid dynamics (CFD) simulation was conducted to investigate and validate the CFD model, which evaluates the heat transfer performance in a spirally corrugated tube that has a twisted tape inserted. The heat transfer was then compared to a simple corrugated tube without the twisted tape and to a smooth tube with no corrugations and no twisted tape.

ACKNOWLEDGMENT

I extend my deepest gratitude to my parents, particularly to my father, whose unwavering support has been a guiding light throughout my doctoral journey. His belief in my abilities, coupled with his constant encouragement and sacrifices, have been the cornerstone of my academic achievements. Dad, your steadfast presence and faith in me until the very end of my PhD mean more to me than words can express.

To my beloved wife, your enduring patience, understanding, and unwavering support have been my greatest source of strength. Your belief in me, even during the most challenging moments, has been a constant inspiration.

Special thanks to my advisor, Samir Moujaes whose guidance and expertise have shaped my scholarly pursuits and led me through the complexities of research.

I am also grateful to my colleagues, friends, and all those who have offered their support and encouragement along the way.

TABLE OF CONTENTS

LIST OF TABLES

LIST OF FIGURES

LIST OF NOMENCLATURE

A	heat transfer surface area, m2
D	tube diameter, m
R	Corrugation radius, m
e	ridge height, m
f	Fanning friction factor
H	pitch of the twisted tape in 360o twist, m
h	heat transfer coefficient, W/(m^2. K)
k	thermal conductivity, W/(m.K)
L	tube length, m
$\dot{m}$	mass flow rate in tube, kg/s
Nu	Nusselt number
p	pitch of ridging, m
Δp	pressure drop, Pa
Pr	Prandtl number
η	Performance factor

$\dot{Q}$	Heat transfer rate, W
Re	Reynolds Number
s	Cap height of the ridge, m
t	Cap width of the ridge, m
ΔT	Temperature difference, K
U	overall heat transfer coefficient, $W/(m^2 . K)$
u,v,w	Velocity components in x,y,z directions respectively, m/s
β	helix angle of rib, deg
B*	$B^* = \beta/90$
φ	Dissipation function
μ	dynamic viscosity, Pa . s
ρ	fluid density, kg/m3
σ	surface tension, kg/s^2

Subscripts

i	inside/inlet, or value at x = 0
m	mean value
o	outside/outlet, or value at x = L
s	smooth tube
w	wall

1. INTRODUCTION AND LITERATURE REVIEW

The use and transfer of energy is necessary in our society today, but that does not come without drawbacks on our planet's environment and our economy. Natural resources are decreasing, as is their cost to produce and transfer. Creating ways to maximize the energy transfer process is extremely valuable and one way to do so is to increase the performance of heat exchangers to reduce energy loss, costs, and materials [1]. One of the best methods to enhance heat transfer in heat exchangers is compound enhancement, which is when different enhancement techniques are used simultaneously. This field is promising for future development [2].

The heat transfer coefficient can be increased significantly using compound enhancement by inserting different devices into a modified tube [2]. The aim of this study is to create a CFD model that is reliable for future attempts at different geometries. Many researchers relied on experiments to develop these enhancements. Heat transfer is increased by corrugation in turbulent flow b increasing the turbulence level and breaking the boundary layer of the flow [3]. Many researchers started using computational methods since these have been developed over recent decades and different computational calculation methods

were created. These new methods allow researchers in saving time and effort, as well as funds that would otherwise be needed to create experimental setups and structures [5]. Sparrow et al (1983). [4] adopted a numerical simulation as early as the 1980s to simulate laminar flow in triangular corrugated tubes and study its heat transfer performance [5].

Corrugated tubes are widely used in heat exchangers, (Chorak et al., 2014) used CFD to investigate the effect of pitch length over the heat transfer. The authors used different pitch distances ranging from 10 to 40mm and an inlet velocity ranging from 0.5 to 2m/s, water is the working fluid. The grooves of the corrugation have a diameter of 1mm, while the temperature on the walls of the tube is 58.6C. The authors pointed out that the diameter of the grooves plays a big role in the turbulence of the flow, the greater the diameter of the grooves is more turbulence is created and hence more heat transfer. Shall the diameter get smaller, the behavior of the flow will look like a smooth tube. The authors predict that the heat transfer is done mainly by free convection when the ratio of the pitch and the groove gets smaller, while it is governed by forced convection when the opposite happens.

Rahman et.al (2013) used FLUENT to investigate the effect of a multi-start inner grooved tube on the flow of refrigerant R22. They found that the enhanced tube provided a higher heat transfer coefficient than smooth tubes.

Rahimi et al. (2009) discuss an experimental and computational fluid dynamics (CFD) investigation on the heat transfer and friction factor characteristics of a tube with modified twisted tape inserts. The study aimed to investigate the effect of different modified twisted tape inserts on heat transfer enhancement and friction factor characteristics. The experimental setup involved a horizontal test section with a heated tube and a modified twisted tape insert. The modified twisted tapes were made of aluminum and had various modifications to the geometrical parameters, such as tape width, twist ratio, and cut angles. The heat transfer coefficient and friction factor were measured experimentally, and CFD simulations were also carried out to validate the experimental results, which showed that the modified twisted tape inserts significantly enhanced the heat transfer coefficient and friction factor compared to the plain tube. Furthermore, the CFD simulations agreed well with the experimental data. The study also investigated the effect of different flow rates on the heat transfer and friction factor characteristics. It was found that increasing the flow rate increased the heat transfer coefficient and friction factor for all the modified twisted tape inserts. In conclusion, the study

showed that the modified twisted tape inserts can significantly enhance the heat transfer coefficient and friction factor of a tube. The results can be useful for the design of heat exchangers and other thermal systems where heat transfer enhancement is important [11].

Lou et al. (2011) conducted a simulation study of heat transfer tubes equipped with twisted-tape inserts, which are commonly used in heat exchangers to enhance heat transfer. The simulations were conducted using computational fluid dynamics (CFD) techniques to investigate the effects of different twisted-tape geometries on heat transfer and fluid flow characteristics. The study found that the twisted-tape inserts significantly enhanced the heat transfer rate in the tubes, with the best results achieved using tapes with a twist ratio of 5 and a width ratio of 0.156. Additionally, the twisted-tape inserts caused an increase in friction factor, which is a measure of the resistance to fluid flow. However, this increase was relatively small and considered a reasonable trade-off for the improved heat transfer performance. Overall, the study highlights the potential of twist-ed-tape inserts as an effective method for enhancing heat transfer in heat exchangers and provides valuable insights into the optimal design of these inserts for different applications [12].

(Salman et al., 2014) ran experiments and numerical simulation to study the effects of the twist ratio and Reynolds number on the heat transfer distribution on a plate heat exchanger. Three twisted tapes were used with twist ratios of 2.93,3.91 and 4.89. Reynolds numbers ranged from 4000 to 16000. The authors conducted numerical simulations using k-omega and k-epsilon models. The k-omega model was more accurate relative to the experiment for a conventional jet, while the k-epsilon was more accurate for the jet with swirls. However, the heat transfer rate was more substantial in the conventional jet than in the jet with twisted tapes, but among the jet with a twisted tape group, the heat transfer was greater with a twist ratio of 4.89 than 2.93 and 3.91.

(Amini et al., 2015) investigated the effect of twisted tapes as well on the heat transfer of impinging jets. The authors focused on 3 parameters, Re ranging from 4000 to 16000, the distance between the jet and the plate with ratios of 2,4,6 and 8, and the twist ratio of the twisted plate ranging from 3 to 6. The optimal conditions were found to be at a jet-to-plate interspace of 6 and 8 and twist ratio of 6. These conditions produced a maximum Nusselt number of just under 100 at a Nusselt number of 16000. However, the authors did notice that the exit velocity dropped by more than half compared to the inlet velocity which point at a high

pressure drop but no further investigation was made to evaluate the energy loss against the heat transfer gain.

(Mat Lazim et al., 2014) found that the impact of spiral corrugation features on overall thermal performance were numerically investigated in this study using two-start spirally corrugated tubes. According to the findings, this shape with smooth spiral corrugations can greatly improve heat transmission at low and medium Reynolds numbers. While the rise in friction factor after Re of 700 is significantly more than the increase in heat transmission, the corrugation profile was found to be the master key for generating better heat transfer with the least amount of pressure drop, and it needed to be adjusted to create more heat transfer with the least amount of pumping power. The severity index u has a significant impact on heat transfer enhancement and friction factor, with heat gained accompanied by pressure loss, particularly at high Re. It was also discovered that this corrugation profile created harmony and ordered swirls in the secondary flow region, lowering pressure drop and saving pumping power.

(Vahidifar and Banihashemi, 2023) studied a simple geometry of turbulators a tube with the disc, ring, and o-ring turbulators with an area ratio equal to the cross section of the turbulator to the pipe (40%) in different pitches. The effect of

stimulating the main air flow in increasing the Nu and thermal performance was investigated. The Nu for the pipe in the presence of turbulators is much higher than that of the smooth pipe in turbulators, and heat transfer increases. By inserting a ring turbulator, the highest value of convection heat transfer coefficient is obtained.

The Nu increases between 2.59 and 3.21 fold at PR = 2 (PR is pitch ratio distancing) for ring, and as the Re increases, so does the heat transfer. The Nu value for the circular ring turbulator is higher than that for the O-ring turbulator, because the vortices' strength, number, and magnitude are important in transferring heat energy. The friction coefficient of the o-ring and circular ring turbulators decreases with the increase of Reynolds number, and the friction coefficient of the circular ring turbulator is higher than that of the o-ring turbulator due to the lack of a streamlined shape and the aerodynamic shape.

Various aspects of shell-and-tube heat exchangers were discussed in (Su et al., 2022), emphasizing the use of U-tube heat exchangers with one tube plate for disassembly convenience and suitability in high-temperature, high-pressure applications. It introduces different baffle designs proposed by researchers,

including quadrant helical baffles and circumferential overlap trisection helical baffles.

A new heat exchanger structure involving special-shaped hole or orifice baffles is presented, aiming to reduce flow resistance, prevent vibration damage, and facilitate tube bundle cleaning. The experimental setup involves heat exchangers with replaceable tube bundle cores, and the testing system uses water in both sides with hot and cold water flowing in the shell-side and tube-side, respectively.

The text details the experimental apparatus, including the testing system, data measurement system, and data control system. It emphasizes the importance of experimental methods in validating simulation models for heat exchangers. The experimental data processing method involves determining fluid properties and analyzing uncertainty.

The performance evaluation section compares helical and segmental baffle schemes, highlighting higher heat transfer coefficients for helical designs. Orifice baffle schemes are shown to outperform segmental baffles, producing a jet effect for enhanced heat transfer. The comparison of different heat exchanger types concludes that helical and orifice baffle schemes exhibit superior overall and shell-

side heat transfer coefficients compared to segmental schemes, with ladder helical schemes slightly outperforming orifice baffle schemes according to comprehensive indexes.

The text in (Gu et al., 2020b) discusses helical flow applications in heat exchangers, particularly focusing on twisted elliptical tube heat exchangers (TETHX). It emphasizes the advantages of TETHX over segmental baffle heat exchangers, highlighting better flow and heat transfer characteristics. Previous studies on TETHX, considering factors such as aspect ratio and twist pitch, are cited.

A new type of TETHX with alternating V-rows of coupling-vortices is proposed to improve heat transfer performance and energy utilization efficiency. The study involves constructing and simulating eleven geometric models, comparing a conventional parallel-vortex structure with the proposed coupling-vortex structure.

The physical model involves a unique tube layout configuration with 37 tubes of a fixed length of 1000 mm and a major axis fixed at 12.3 mm. The hydraulic diameter of the tube bundle is defined as the cross-sectional area on the shell side multiplied by four.

The simulation results are validated against experimental correlations, and the analysis includes velocity, pressure, and temperature fields. The unique coupling-vortex technology is proposed as an effective enhancement for TETHX without additional manufacturing costs.

Comprehensive performance analysis considers Nusselt number, friction factor, and a comprehensive index. The study concludes that the coupling-vortex schemes in TETHX exhibit higher heat transfer coefficients, slightly higher pressure drops, and more uniform temperature fields compared to parallel-vortex schemes. The mean values for the coupling-vortex schemes are reported as 7.8%, 8.7%, and 4.9% for heat transfer coefficients, pressure drops, and temperature field uniformity, respectively. The unique coupling-vortex technology is suggested as a promising enhancement for TETHX with improved thermal and hydraulic performance.

The study made by (Li et al., 2021) delves into the intricacies of shell-side convection heat transfer and hydraulic resistance in double tube heat exchangers (DTHEs) employing twisted oval tubes (TOTs). Notably, the research identifies Case 10 as yielding the highest comprehensive heat transport performance.

In the realm of double tube heat exchangers, renowned for their widespread application in diverse industries, the investigation concentrates on the deployment of twisted oval tubes (TOTs). This choice stems from the notable heat transfer performance exhibited by TOTs, prompting a departure from previous studies primarily focused on high Reynolds numbers. Instead, this research deliberately explores the dynamics at play in low Reynolds number flow scenarios.

The physical model under scrutiny involves DTHE configurations featuring coaxial TOTs and circular tubes (CTs). The investigation encompasses 14 distinct cases, each characterized by unique geometric dimensions. To facilitate clear communication, a nomenclature is introduced, aiding in the systematic description and differentiation of the various DTHE configurations.

Employing a sophisticated 3-D computational model, the study meticulously scrutinizes the heat transport and hydraulic resistance properties within the shell side of DTHEs. The turbulent regime is captured using the SST k-w turbulent model, and a comprehensive performance evaluation criterion (PEC) becomes the yardstick for assessing the multifaceted performance metrics.

Prior to delving into the specifics of the investigation, the study ensures the independence of the computational grid and validates the numerical model. The

SST k-w turbulent model emerges as the most fitting choice for capturing the nuanced behavior of twisted oval tubes. Validation exercises demonstrate a commendable alignment between numerical simulations and experimental data.

Scientific insights gleaned from the results shed light on critical aspects:

- Aspect Ratio (A/B): DTHEs featuring TOTs exhibit heightened heat transfer advantages when the outer aspect ratio (Ao/Bo) is maintained below 1.60.
- Twisted Pitch Ratio (P/de): Smaller P values foster enhanced turbulence, resulting in heightened heat transfer performance.
- Twisting Direction: Surprisingly, the twisting direction does not wield a substantial impact on either heat transport or hydraulic resistance.
- Diameter Ratio (di/do): Instances where DTHEs incorporate TOTs as inner tubes and CTs as outer tubes reveal varying di/do values, influencing the effectiveness of heat exchange from the inner tube wall to the surrounding water.

In conclusion, the study illuminates the substantial augmentation of heat transport performance achievable in DTHEs through the strategic integration of TOTs and CTs. The observed enhancements range from 24.0% to 39.0%, underscoring the potential of this configuration. Additionally, it becomes evident

that manipulating the inner aspect ratio (Ai/Bi) exerts a more discernible influence on performance than variations in the outer aspect ratio (Ao/Bo).

(Pirbastami and Moujaes, 2016) presents a Computational Fluid Dynamics (CFD) study on heat enhancement in helically grooved tubes. The study explores the impact of different groove dimensions on the thermal performance and pressure drop of water inside grooved tubes. The authors investigate three rectangular grooved tubes with varying groove width (w) and depth (e) and analyze the Reynolds number (Re) range of 4000-10000. The results show that the highest performance is achieved with specific groove dimensions (w=0.2 mm and e=0.2 mm). Additionally, the study examines the influence of pitch size to tube diameter (p/D) ratios on Nusselt number (Nu) and friction factor (f). The findings indicate that increasing the p/D ratio leads to a decrease in both Nu and f values. The paper provides empirical correlations for Nu and f as functions of p/D and Re number, suggesting that incorporating internal grooves with specific dimensions can enhance heat exchanger performance.

1.1 RESEARCH OBJECTIVES

The primary objective of this work is to investigate the effect of geometrical parameters on the heat transfer of heat exchangers with water as the working fluid.

This study is based on the experimental work presented in Zimparov et .al (2012) where the authors tested a range of different geometries under different boundary conditions that will be covered later in this manuscript. Subsequently, it is also the intent of this study to try to find a geometry that improves the performance than what already exists in the literature. A secondary objective of this work will be to take advantage of the numerical simulations to investigate flow characteristics that would not be possible using purely experimental work such as the relation between the turbulent kinetic energy, pressure drop, and the heat transfer. This work is structured as follows:

- Create and Validate a CFD model using experimental data.
    - Create a CAD model identical to the geometry in Zimparov et.al (2012) using SolidWorks.
    - Import the CAD model into the CFD simulation software STAR-CCM+ to conduct a grid independence study. The grid independence study will rely on comparing flow parameters such as Axial temperature and Axial velocity at different mesh sizes. Once the change in the results is no longer significant (<2-3%), it can be assumed that grid independence was achieved.

- Validate the CFD model with the experimental data from Zimparov et.al (2012) by running simulations for all the 16 different boundary conditions that will be detailed later in this text.
- Establish the metric $\eta = \frac{\frac{Nu}{Nu_S}}{\frac{f}{f_S}}$ to evaluate the gain in heat transfer against the loss of energy due to the pressure drop.

- Introduce a new geometry.
  - Create a new geometry using SolidWorks whose purpose would be to enhance the η factor by either increasing the heat transfer/reducing the pressure drop or both.
  - This new geometry will be made of sets of vanes mounted on a 1m long shaft and inserted inside a simple tube of 12 mm diameter.
  - Varied spacing between each set of vane will be tested to try to find the best dimensions (i.e. 5 cm, 7.5 cm, 10 cm, 12.5 cm).
  - Test the new geometry under the same BCs from Zimparov et.al (2012), compute the factor η, and assess any improvements.

2. NUMERICAL METHOD AND PROCEDURE

As mentioned above the simulation results are compared with a previous experimental study conducted by (Zimparov et al. 2012), which focuses on tubes with a height-to-diameter ratio e/Di > 0.04 and small relative pitches of the twisted tape, H/Di. The largest improvement was noticed in the tube with e/Di= 0.057 (Tube 5035) and ridge pitch-to-height ratio p/e=6.77 with a twisted tape of H/Di= 4.7. Tube 5035 was found to have the most significant enhancement, hence the focus of the CFD simulation will be on this tube, and the simulation will range for Reynolds numbers, $3.5 \times 10^3 < Re < 5.0 \times 10^4$. The focus of this simulation is the evaluation of heat transfer and friction factors; a metric η was used to obtain an empirical representation of the tube's performance.

The new geometry will have a similar concept as the tube 5035. It is made of a tube and an insert, the insert being 21 sets of vanes mounted on a 1 m long shaft as presented later in the manuscript.

The aim of this section is to create the CFD model that will try to replicate the experiment and results presented in Zimparov et .al (2012). To achieve that the first step will be to recreate the geometries of tube 5030 and tube 5035 as a CAD model.

Once the geometries are created, it can then be imported into the simulation software STAR-CCM+. A grid independence study will need to be done before subjecting those geometries to the same flow and boundary conditions from Table 2 and 3.

2.1 HEAT EXCHANGER MODEL

The 3D models were made in SolidWorks according to the dimensions provided in Table 1.

Figures 1 and 2 shows the model for tube 5030 where the ridge can be noticed. We also notice the absence of the twisted plate.

Figures 3 and 4 shows the model for tube 5035 where we can notice the twisted plate of pitch 4.7 inserted in the corrugated tube.

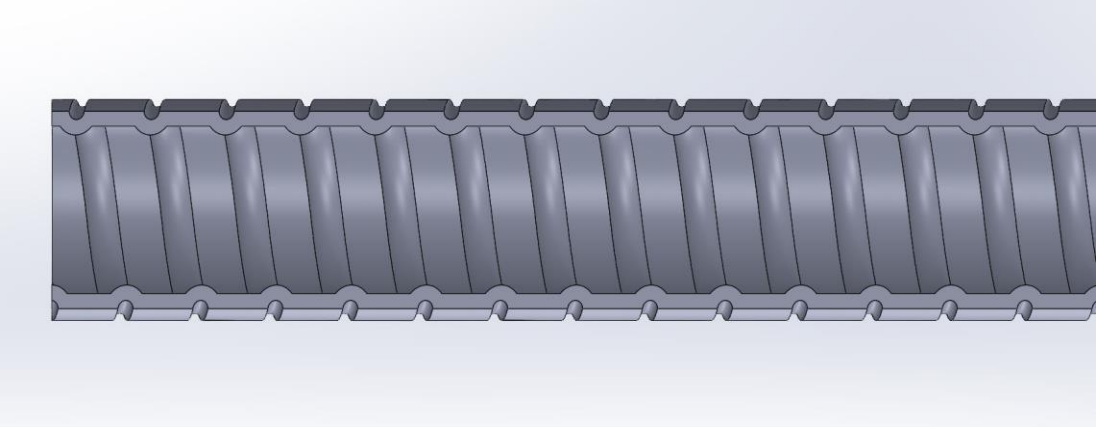

Figure 1 Cross section view of tube 5030.

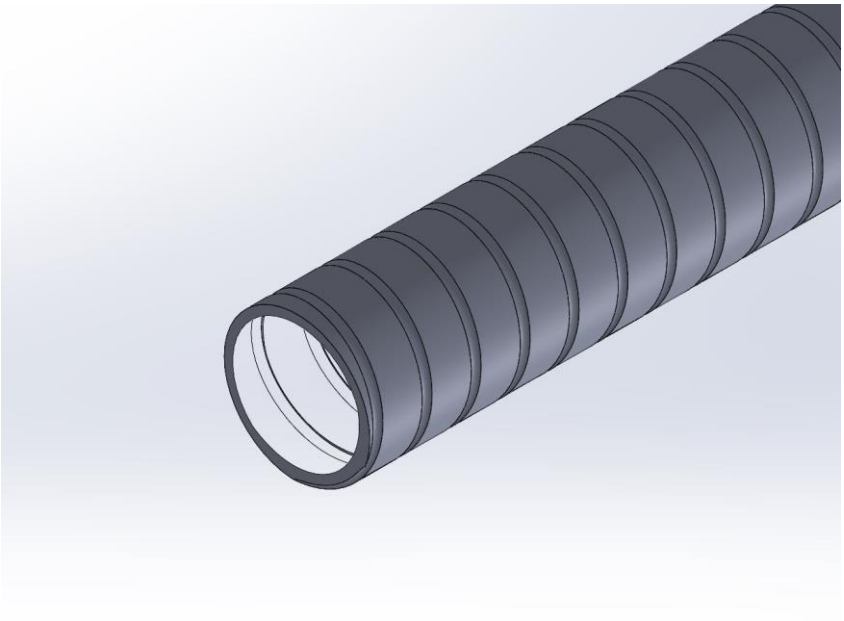

Figure 2 Isometric View of tube 5030.

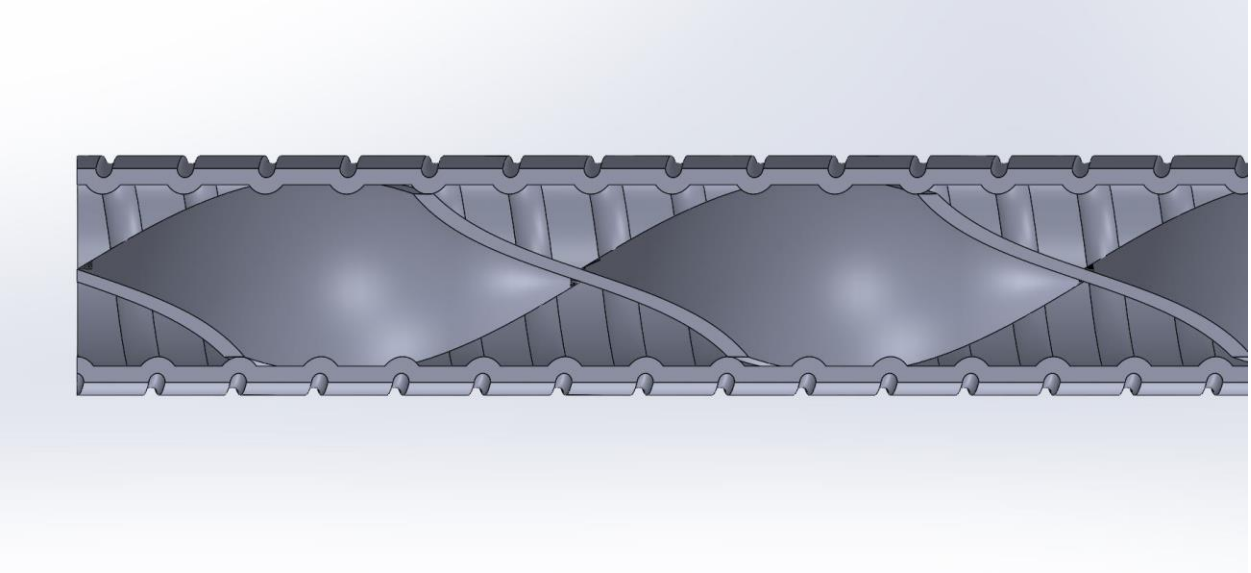

Figure 3 Cross-section view of tube 5035.

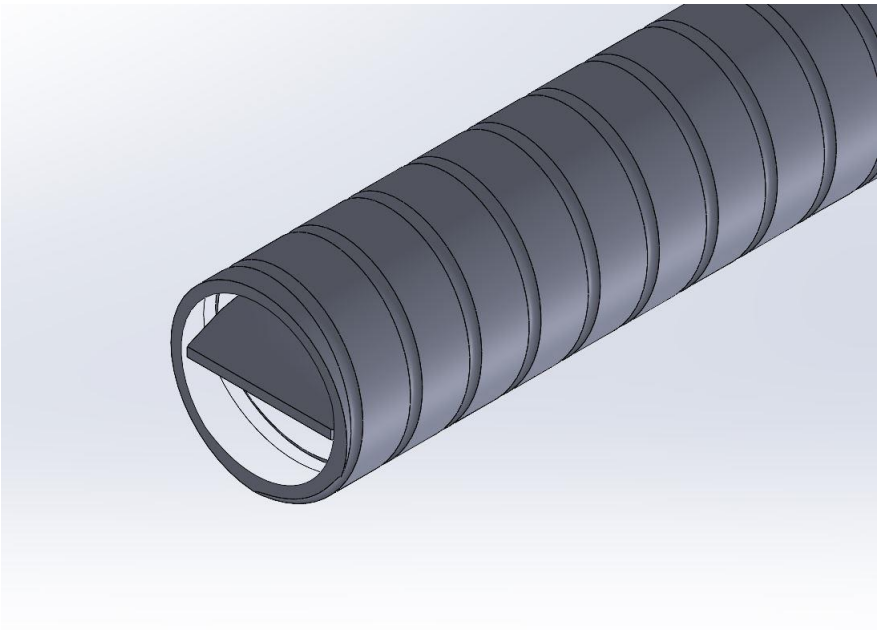

Figure 4 Isometric view of tube 5035.

2.2 GOVERNING EQUATIONS AND TURBULENCE MODEL

This study focuses on turbulent flow at a range of Reynolds number of 3.5 x 10^3 < Re < 5.0 x 10^4, and the twisted plate mixes the flow and adds turbulence.

The governing equations of this simulation are the incompressible Reynolds averaged Navier-Stokes equations, the energy equation, and the steady 3-D form of the continuity.

Conservation of mass:

$$\boldsymbol{\rho \nabla \cdot \overline{V} = 0} \tag{5}$$

Navier-Stokes equations:

$$\boldsymbol{\rho\left(\overline{u}\ \frac{\partial \overline{u}}{\partial x} + \overline{v}\ \frac{\partial \overline{u}}{\partial y} + \overline{w}\ \frac{\partial \overline{u}}{\partial z}\right) = \rho g_x - \frac{\partial \overline{p}}{\partial x} + \mu\left[\frac{\partial \overline{u'u'}}{\partial x} + \frac{\partial \overline{u'v'}}{\partial y} + \frac{\partial \overline{u'w'}}{\partial z}\right]}$$

(x direction) (6)

$$\boldsymbol{\rho\left(\overline{u}\ \frac{\partial \overline{v}}{\partial x} + \overline{v}\ \frac{\partial \overline{v}}{\partial y} + \overline{w}\ \frac{\partial \overline{v}}{\partial z}\right) = \rho g_y - \frac{\partial \overline{p}}{\partial y} + \mu\left[\frac{\partial \overline{v'u'}}{\partial x} + \frac{\partial \overline{v'v'}}{\partial y} + \frac{\partial \overline{v'w'}}{\partial z}\right]}$$

(y direction) (7)

$$\boldsymbol{\rho\left(\overline{u}\ \frac{\partial \overline{w}}{\partial x} + \overline{v}\ \frac{\partial \overline{w}}{\partial y} + \overline{w}\ \frac{\partial \overline{w}}{\partial z}\right) = \rho g_z - \frac{\partial \overline{p}}{\partial z} + \mu\left[\frac{\partial \overline{w'u'}}{\partial x} + \frac{\partial \overline{w'v'}}{\partial y} + \frac{\partial \overline{w'w'}}{\partial z}\right]}$$

(z direction) (8)

Conservation of Energy:

$$\nabla . k\nabla T + \mu\varphi = 0 \tag{9}$$

Dissipation function:

$$\varphi = 2\left[\left(\frac{\partial u}{\partial x}\right)^2 + \left(\frac{\partial v}{\partial y}\right)^2 + \left(\frac{\partial w}{\partial z}\right)^2\right] + \left(\frac{\partial u}{\partial y} + \frac{\partial v}{\partial x}\right)^2 + \left(\frac{\partial v}{\partial z} + \frac{\partial w}{\partial y}\right)^2 + \left(\frac{\partial w}{\partial x} + \frac{\partial u}{\partial z}\right)^2 \tag{10}$$

The CFD model used is the k-ε model. In the k–ε two equation model, the velocity and length scale of turbulence are defined with two additional partial-differential equations: one for the turbulent kinetic energy k, the other for the dissipation rate ε, and an algebraic demonstration for the eddy viscosity.

Kinetic energy Equation k:

$$\boldsymbol{\rho\langle u_j\rangle \frac{\partial k}{\partial x_j} = 2\mu_t\langle s_{ij}\rangle \frac{\partial\langle u_i\rangle}{\partial x_j} - \rho\varepsilon + \frac{\partial}{\partial x_j}\left[\left(\mu + \frac{\mu_t}{\sigma_k}\right)\frac{\partial k}{\partial x_j}\right]} \tag{11}$$

Dissipation rate equation $\boldsymbol{\varepsilon}$**:**

$$\boldsymbol{\rho\langle u_j\rangle \frac{\partial \varepsilon}{\partial x_j} = C_{\varepsilon 1} P_k \frac{\varepsilon}{k} - C_{\varepsilon 2}\rho\frac{\varepsilon^2}{k} + \frac{\partial}{\partial x_j}\left[\left(\mu + \frac{\mu_t}{\sigma_\varepsilon}\right)\frac{\partial \varepsilon}{\partial x_j}\right]} \tag{12}$$

Eddy Viscosity:

$$\boldsymbol{\mu_t = C_\mu \rho \frac{k^2}{\varepsilon}} \tag{13}$$

where:

p = density of air

k = turbulence kinetic energy

s_{ij} = rate of dissipation

x_i, x_j = coordinate

u_i = mean velocity

μ = viscosity

μ_t = turbulent viscosity

σ_k, σ_ε = turbulent Prandtl number for k and s

C_μ, $C_{\varepsilon 1}$, $C_{\varepsilon 2}$ = Constants.

The constant variables of k–ε were suggested by STARCCM+ software as follows [1]: $C_\mu = 0.09$, $C_{\varepsilon 1} = 1.44$, $C_{\varepsilon 2} = 1.92$, $\sigma_k = 1.3$ and $\sigma_\varepsilon = 1$.

The k–ε is the most widely used and validated turbulence model with applications ranging from industrial to environmental flows. It is known for its reasonable accuracy and economy when it comes to computing power.

The standard k–ε model is suitable only for fully turbulent due to the assumption in its the derivation that the flow is fully turbulent and the effects of molecular viscosity are negligible. The molecular viscosity is the resistance measure of a fluid to deform. The experiment in this manuscript fits these assumptions, as the Re is in the turbulent range and the working fluid is water which allows us to neglect the molecular viscosity.

2.3 GRID INDEPENDENCE STUDY

The first step before starting to generate results in a CFD simulation is to determine an appropriate mesh size for the model that will give us accurate results and not use too much computing power unnecessarily. The density of the grid will vary until the variation of the results between one grid density and another larger one does not vary by more than one or two percent. Once grid independence is satisfied, the next step would be to compare the CFD results with the experimental one.

The two parameters that will be compared throughout the grid independence study are axial velocity and axial temperature along the outlet diameter. Figure 5 shows a probe line along the outlet diameter.

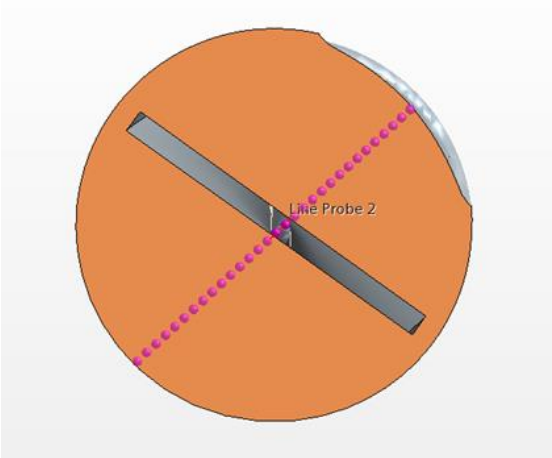

Figure 5 Probe line along the outlet diameter for axial velocity and temperature results.

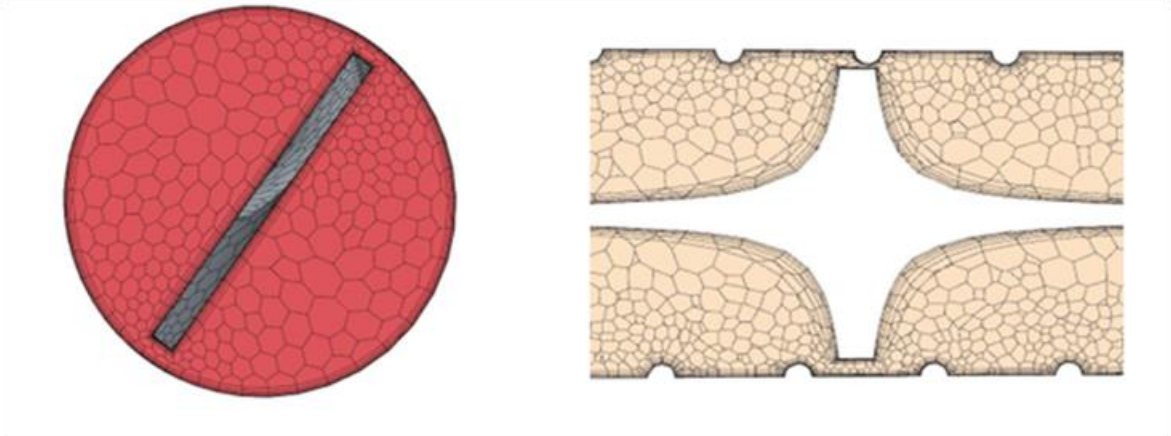

Figure 6 Volume mesh and prism layer at the walls

A polyhedral mesh was used. Its main advantage is that each element has many adjacent cells, which helps reduce errors in gradients. Polyhedrons are also less susceptible to stretching than tetrahedrons, resulting in enhanced mesh quality and model numerical stability. A prism layer was also used at the walls of the tube to capture the change of the temperature gradient in the boundary layer. Figure 6 shows the prism layer with a total thickness of 10% of the mesh size.

Four grids were tested: grid 1: 1,250,789 elements; grid 2: 2,603,124 elements; grid 3: 3,762,700 elements; and grid 4: 5,341,023.

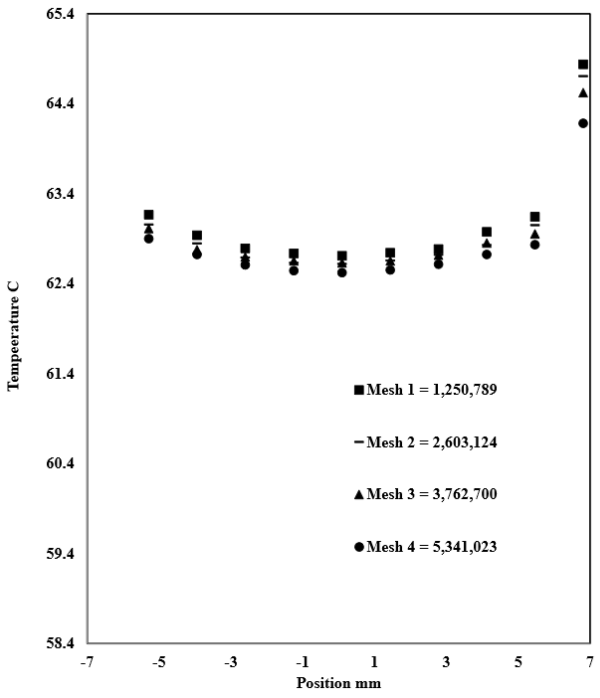

Figure 7 Axial temperature for four different meshes along the outlet diameter of the pipe.

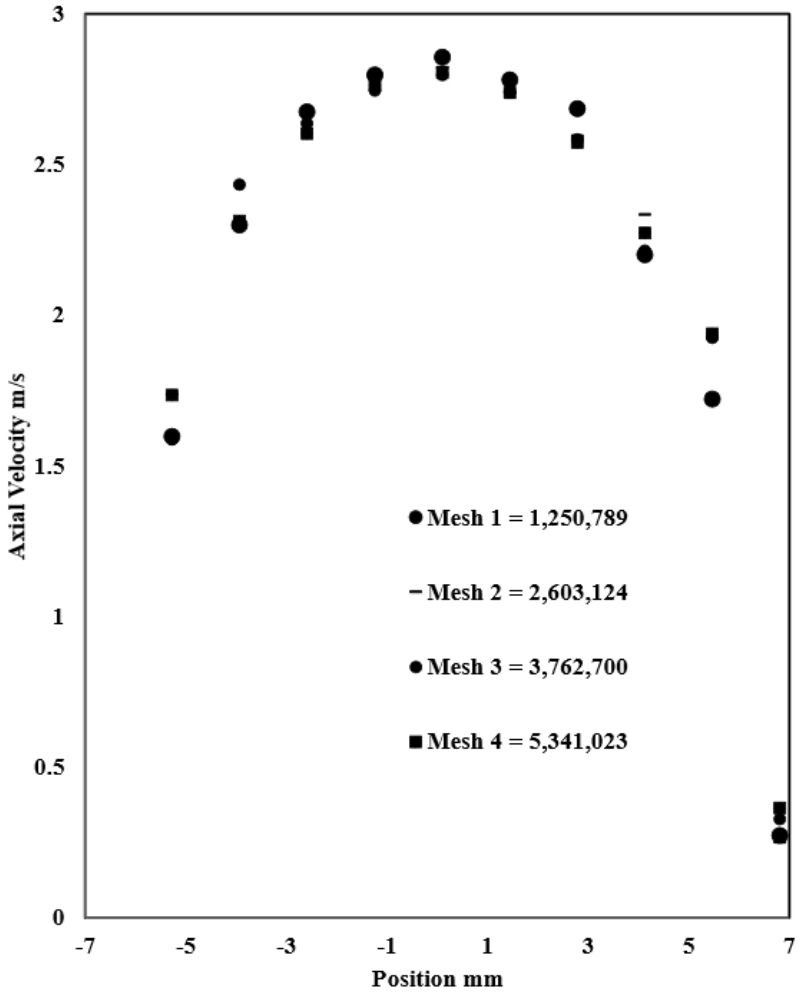

Figure 8 Axial velocity for four different meshes along the outlet diameter of the pipe.

From Figure 7 and 8 we can notice that the change is minimal between mesh size 4 and 3. Since mesh size number 3 has less elements, that will be the base size for the rest of this work which is 3 mm.

3. EXPERIMENTAL EVALUATION OF TUBULAR HEATEXCHANGER WITH TWISTED TAPE INSERT.

3.1 INTRODUCTION AND EXPERIMENTAL SETUP

In 2012 Zimparov et.al conducted an experimental evaluation of one of the most promising heat transfer enhancement techniques - compound enhancement. The experiment comprised eight spirally corrugated tubes made from copper with different geometrical parameters, combined with three twisted tapes with different pitches. The tubes are 1.2 m long.

The three twisted tapes have been defined with three different numerals referring to the pitch of each twisted tape. 0 – corrugated tube alone; 3 – H/D_i = 7.6; 4 – H/D_i = 5.7 and 5 – H/D_i = 4.7. For example, tube 5030 has no twisted tape inserted, tube 5035 has a twisted tape of H/D_i = 4.7. All the twisted tapes are 12.5 mm in width and 0.8 mm in thickness.

A smooth tube was used to standardize the experimental setup and will be used for comparison purposes of the enhancement in heat transfer and pressure drop. FIG.1 shows a schematic of the experimental setup.

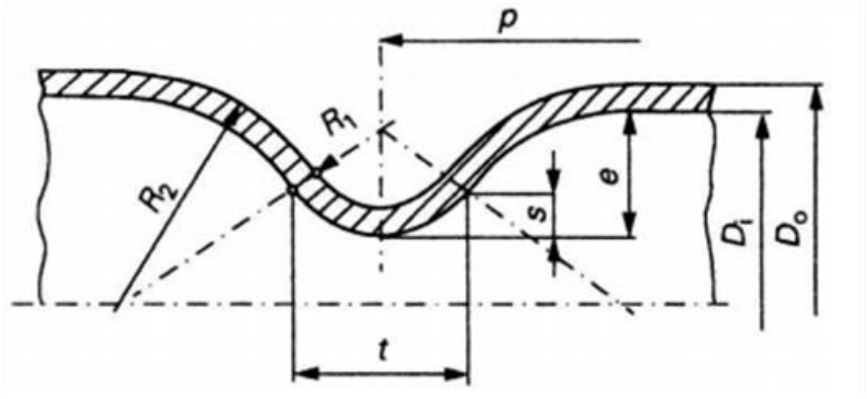

Figure 9 Picture showing the geometrical parameters presented in Table 1. Zimparov et.al (2012)

Figure 9 shows the different geometrical parameters of the corrugations and twisted tape. More details on these parameters are represented in Table 1.

Tube 5035 had the highest heat transfer enhancement out of the 8 other variations; hence this study is focusing on that geometry while tube 5030 will be used for comparison to show the effect of the twisted tape.

Table 1 Geometric parameters of tubes 5030 and 5035

No	D_o mm	D_i mm	e mm	p mm	β deg	t mm	s mm	e/D_i	p/e	B*	Twisted tape
5030	15.31	13.51	0.767	5.19	83.0	1.836	0.371	0.057	6.77	0.922	N/A
5035	15.31	13.51	0.767	5.19	83.0	1.836	0.371	0.057	6.77	0.922	H/Di=4.7

3.2 BOUNDARY CONDITIONS AND EXPERIMENTAL RESULTS

Table 2 Boundary Conditions for 5030

Run	Re	Vi (m/s)	Ti (C)	Tw (C)
1	2590	0.170482	26	43.1
2	3540	0.233013	28.4	43.4
3	4400	0.289621	30.9	43.3
4	4750	0.312659	32.6	44
5	5900	0.388356	34.8	45.4
6	7030	0.462736	36.5	45.9
7	8440	0.555546	38.6	49.3
8	9420	0.620053	40.8	52
9	11860	0.780661	43	52.7
10	14340	0.943902	45.4	53.8
11	17840	1.174283	47.9	54.9
12	21090	1.388207	50.4	56.5
13	28870	1.90031	58.4	64
14	33010	2.172818	67	74.4
15	37170	2.446641	76.4	83.6
16	42060	2.768516	86	91.6

Table 3 Boundary Conditions for 5035

Run	Re	Vi (m/s)	Ti (C)	Tw (C)
1	2220	0.146111	23.5	38
2	3180	0.209294	27.7	41
3	4110	0.270502	30	41.4
4	4850	0.319206	32.8	43.2
5	5760	0.379098	35	44.1
6	4260	0.280375	37.3	45
7	8540	0.562066	39.6	47.55
8	10500	0.691064	42.1	50.9
9	12050	0.793079	44.4	52.1
10	14560	0.958276	46.4	52.8
11	17840	1.174151	48.8	55.1
12	21540	1.417669	51.1	56.95
13	29570	1.946169	60.1	63.5
14	34280	2.256161	69.5	76.05
15	38240	2.516791	78.5	84.62
16	41620	2.739248	86.1	91.8

The experiment consisted of 16 different boundary conditions for each tube variation. Reynolds number spanned from the high transitional flow values to fully turbulent $2.2x10^3 < Re < 5x10^4$, with varied inlet speed, inlet water temperature and wall temperature. Table 2 and 3 contains more details about the boundary conditions.

The two parameters of interest in investigating in this study are the Heat transfer coefficient and the friction factor. The inside heat transfer coefficient h_i is represented as a function of Nu with the following relation:

$$\boldsymbol{N_u = \frac{h_i Di}{k}} \quad (1)$$

While h_i is:

$$\boldsymbol{h_i = \frac{\dot{Q}}{A_i \Delta T_m}} \quad (2)$$

$$\boldsymbol{\Delta T_m = \frac{T_0 - T_i}{lnln\left(\frac{Tw,m - T_i}{Tw,m - T_0}\right)}} \quad (3)$$

The fanning friction factor is given by:

$$\boldsymbol{f = \frac{\rho \pi^2 Di}{32L} \frac{\Delta P}{\dot{m}^2}} \quad (4)$$

Table 4 Uncertainties of measured and calculated parameters.

Parameter	Uncertainty
Water and steam temperature Ti, To,Ts	± 0.1%
Mean tube wall temperature, Tw	±0.5%
Pressure drop, ΔP	±5.0%
Mass flow rate of water, ṁ	±2.0%
Fanning friction factor, f	±6.5%
Cendensing heat transfe coefficient, ho	±2.5%
Inside heat transfer coefficient, hi	±(15-20)%

Table 4 provided by Zimparov et al. represents the errors of the calculated parameters, which will be useful to validate the CFD model, as the goal is to have the CFD results fall within those margins of errors.

3.3 MODEL VALIDATION

To make sure the CFD model is correct, comparing the simulation results against experimental data is necessary before conducting any further studies. The uncertainties from experimental measurement are represented by error bars (Table 6). The same boundary conditions from the experiment (Tables 2 and 3) were used in the CFD simulation.

The properties of interest in this study are the Nusselt Number and the friction factor which are two dimensionless entities of the heat transfer and pressure drop respectively.

3.3.1 HEAT TRANSFER COEFFICIENT

The heat transfer coefficient calculated is an average value on the inside walls of the tube. Fig. 10 and 11 show that the heat transfer coefficient increases

with the Re number, and that the CFD results exhibit the same behavior as the experimental data.

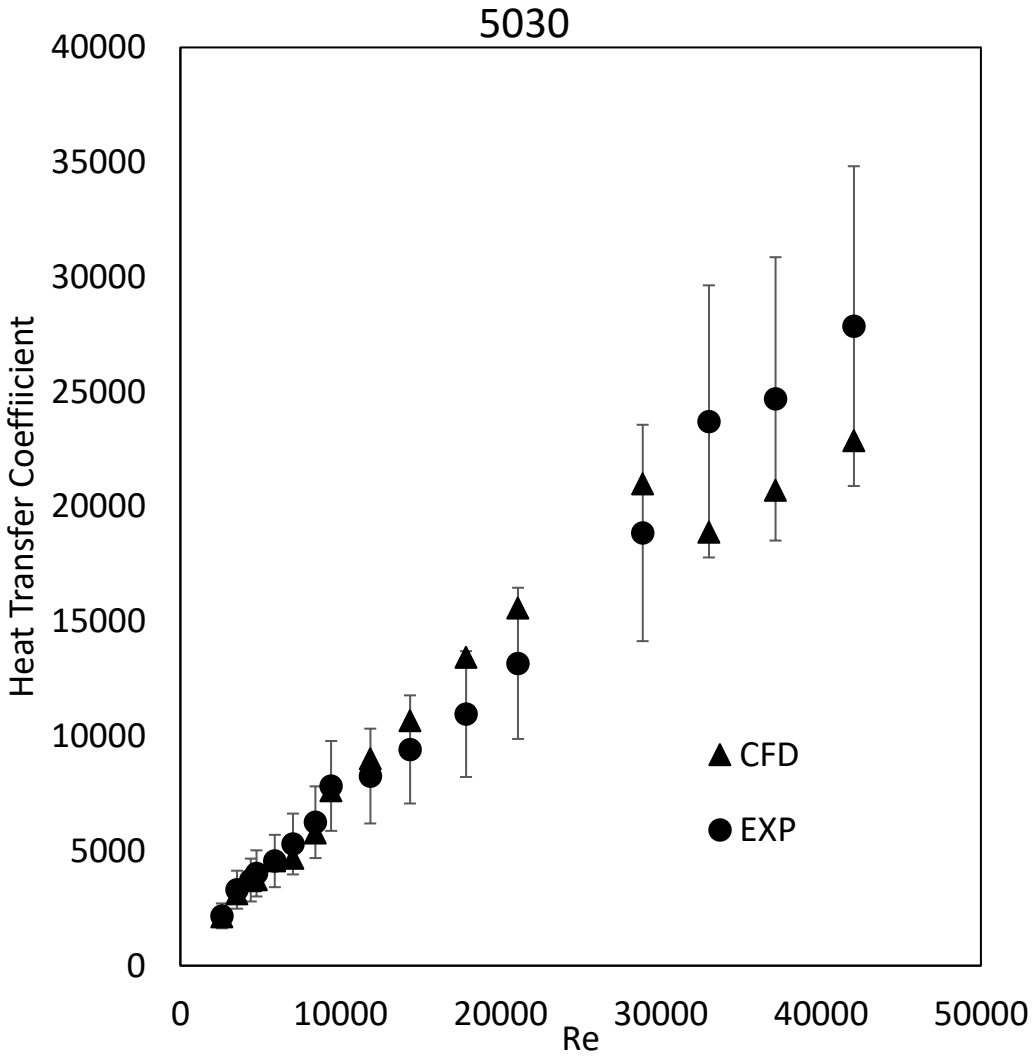

Figure 10 Comparison of Heat Transfer factor obtained from CFD simulation with experimental data for tube 5030.

The calculation was made by implementing equations 2 and 3 as a field function in STAR-CCM+, while the area and the heat transfer were calculated by the software automatically. As expected, the heat transfer is increased in tube 5035 due to the additional heat conduction provided by the plate insert. The error bars are obtained from the measurement of Zimparov (2012).

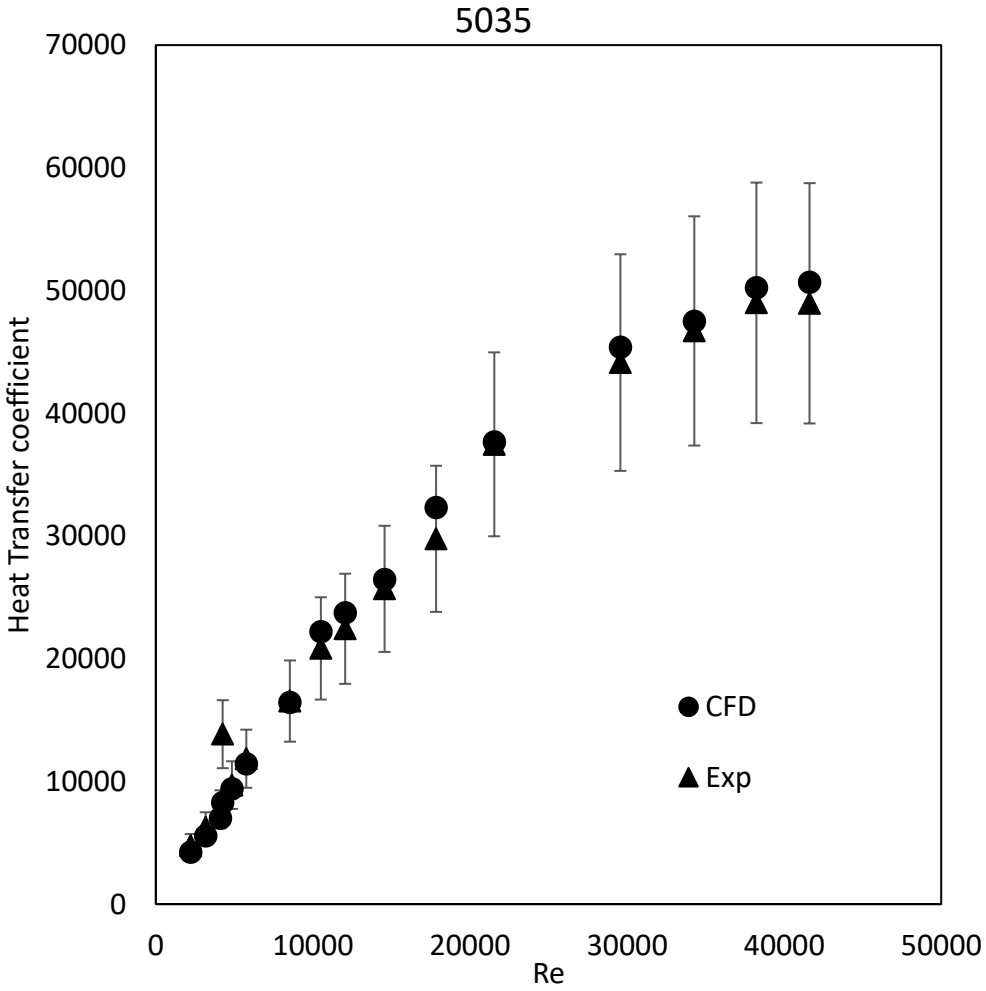

Figure 11 Comparison of Heat Transfer factor obtained from CFD simulation with experimental data for tube 5035.

The CFD results agree with the experimental ones and are within the error bars based on table 2, indicating that the CFD model is accurate enough.

3.3.2 FRICTION FACTOR

The friction factor was also calculated by implementing equation 4 into the software, while the area, mass flow rate, and pressure drop were calculated automatically from STAR-CCM+.

Here again, the CFD results agree with the experimental results as shown in Fig. 12 and 13 for tubes 5030 and 5035.

As expected, the friction factor increased substantially in tube 5035 due to the added friction by the twisted plate. This means that there is an increase in head loss, which will require more pumping power to get the water from one end to another.

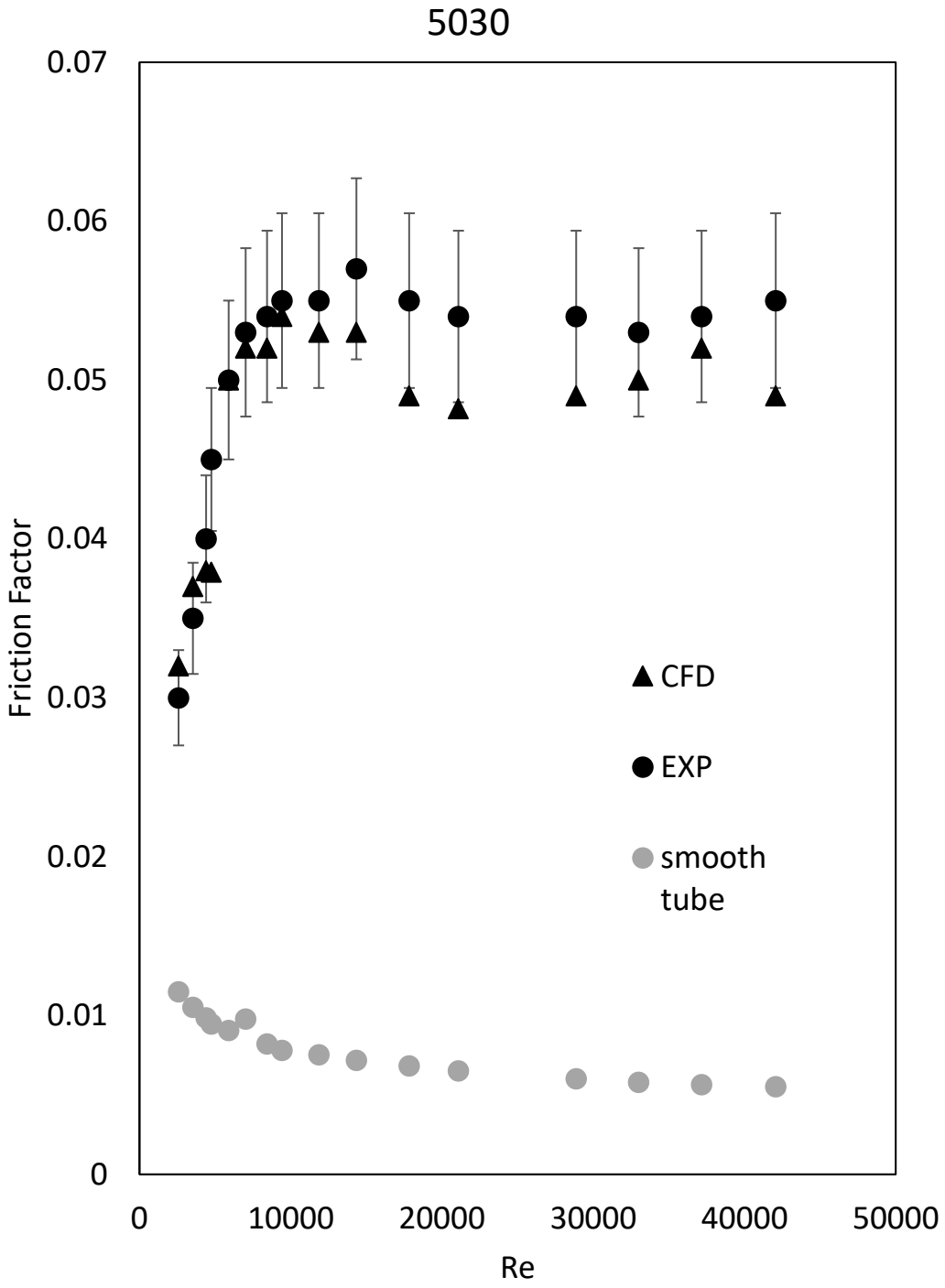

Figure 12 Comparison of friction factor obtained from CFD simulation with experimental data for tube 5030.

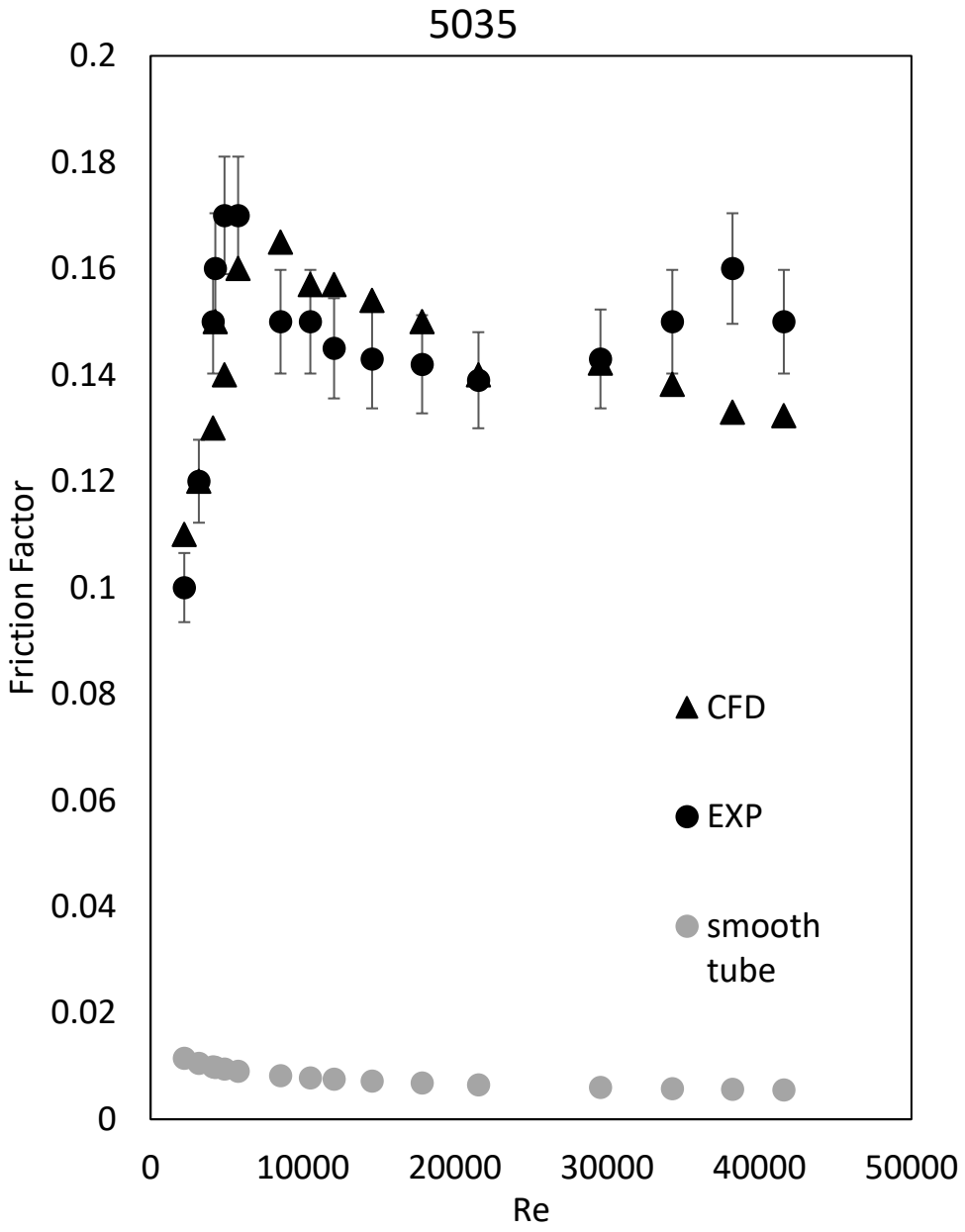

Figure 13 Comparison of friction factor obtained from CFD simulation with experimental data for tube 5035.

3.3.3 NUSSELT NUMBER

In Zimparov et.al (2012) the heat transfer quantification was represented as the product of the Nusselt Number (equation 1) and the Prandtl number of water at different temperatures as $Nu.Pr^{-0.4}$.

To keep similarity with that data the same equation was used to collect the values from the CFD simulation.

For both tubes 5030 and 5035, the Nusselt number kept increasing with Re as shown in Fig.14 and 15. Tube 5035 has a Nusselt number two times higher than tube 5030 due to the increased heat transfer caused by the inserted tape .

The CFD values for $Nu.Pr^{-0.4}$ are within the error range, thus we can conclude that the model predicted the experimental results accurately and hence it is validated.

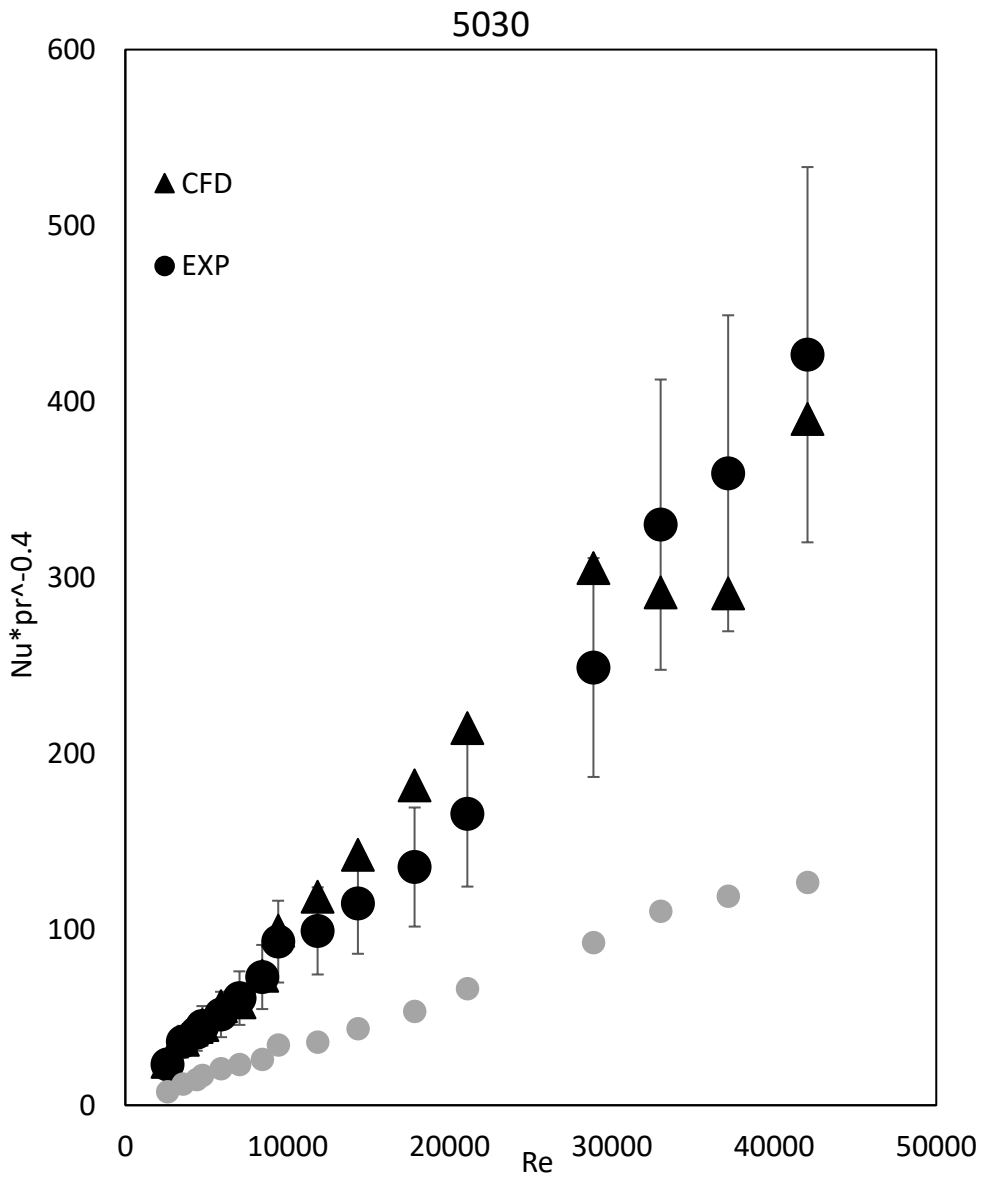

Figure 14 Comparison of Nusselt number obtained from CFD simulation with experimental data for tube 5030.

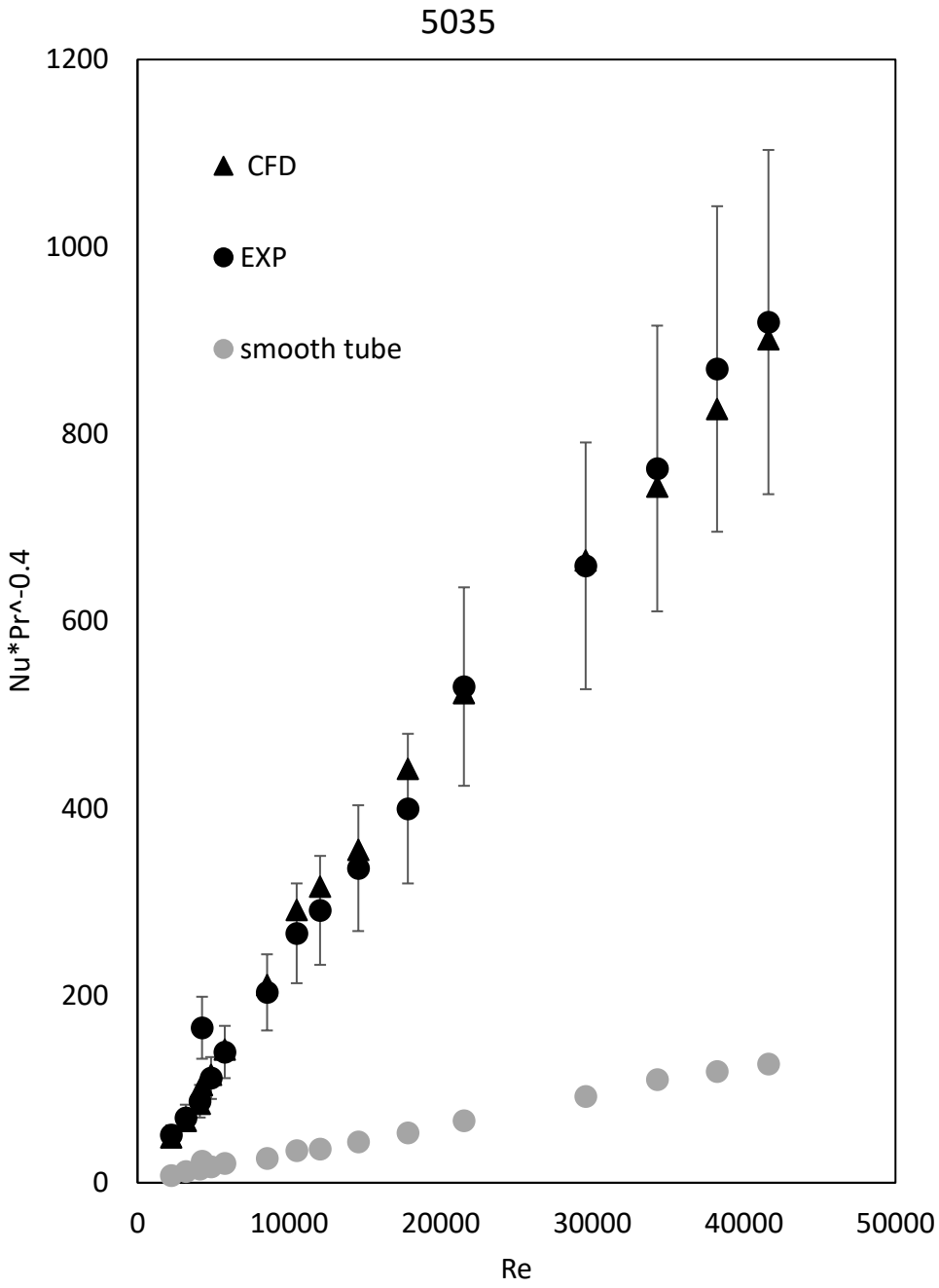

Figure 15 Comparison of Nusselt number obtained from CFD simulation with experimental data for tube 5035.

3.4 THERMAL PERFORMANCE

As mentioned previously, there was an increase in the amount of heat conducted by the twisted plate, but that comes with more friction caused by the plate's geometry, which results in head loss as discussed in section 3.4.2.

The goal here is to increase the heat transfer without increasing the pressure drop to a level where it is no longer beneficial due to the required pumping power.

$$\boldsymbol{\eta} = \frac{\frac{\boldsymbol{Nu}}{\boldsymbol{Nus}}}{\frac{\boldsymbol{f}}{\boldsymbol{fs}}} \tag{14}$$

The enhancement factor η will allow us to evaluate the gain in heat transfer against the energy loss where Nu/Nu_s is the ratio of the Nusselt number of the smooth tube and 5035, and f/f_0 is the ratio for the fanning factor.

These ratios Nu/Nu_s and f/f_s are a dimensionless representation of the heat transfer and pressure drop, respectively, that allows for the comparison of both properties. Other papers have used a similar factor such as (Shaver et al., 2019) and (Wu et al., 2018).

If $\eta<1$, that means that the friction factor is greater than the heat transfer, indicating that the tube's design is not efficient for transferring heat without increasing the cost of energy consumption required for pumping.

On the other hand, if η ≥ 1, the tube design can be used for enhancement purposes.

Table 5 η factor between tubes 5035 and smooth tube for experimental and CFD values.

$\eta = \frac{Nu5/Nus}{f5/fs}$	
CFD	EXP
0.6480932	0.753533
0.4786437	0.503545
0.4350044	0.389741
0.4564574	0.364399
0.3877472	0.358266
0.2935751	0.436242
0.4029665	0.426955
0.4224512	0.404242
0.4218259	0.420342
0.3809164	0.387688
0.3772454	0.360315
0.3674824	0.375098
0.304549	0.300184
0.2829842	0.26754
0.2952993	0.258176
0.2971056	0.267389

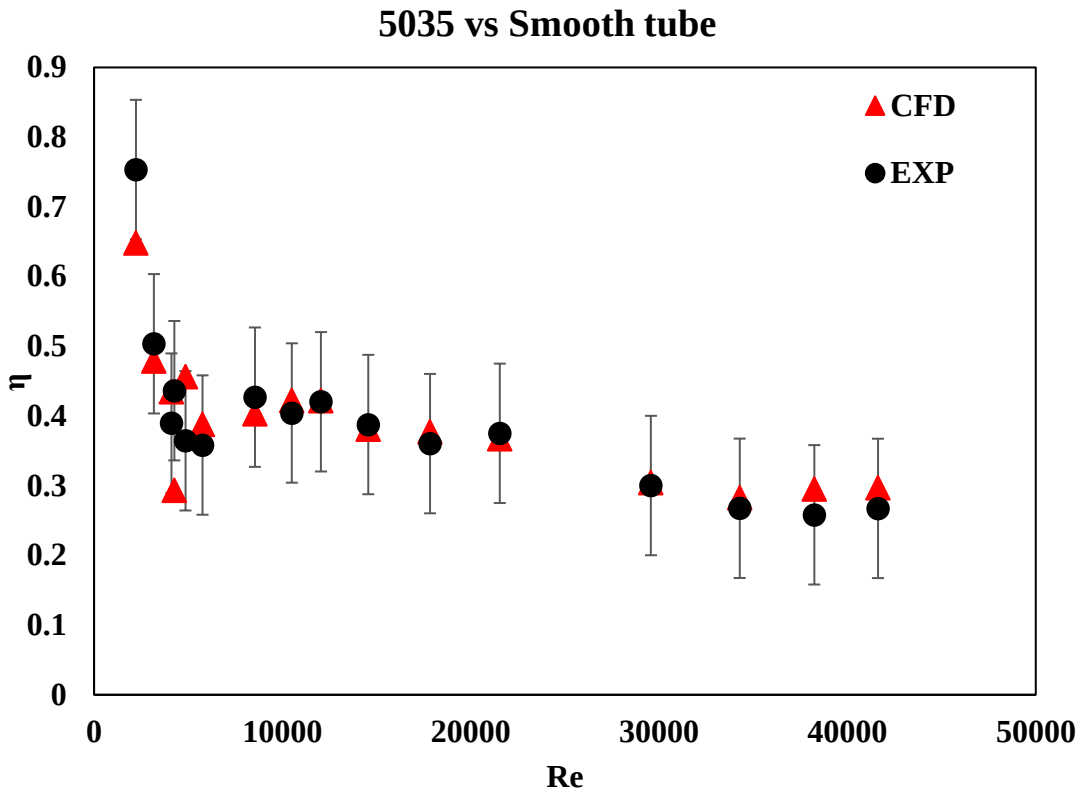

Figure 16 Enhancement factor η comparing the performance of tube 5035 with smooth tube.

Table 6 shows a comparison of the η values calculated from the experimental and the CFD values. It can be noticed that accuracy ranged from 2% to 20% which showcases the accumulated uncertainties from the experimental values.

Figure 16 gives a nuanced look at these results once the error bars are included which considers the uncertainties from table 6.

3.5 TURBULENT KINETIC ENERGY AND HEAT TRANSFER

One of the benefits of numerical analysis is the ability to investigate and showcase certain properties that would be very challenging to do in an experimental investigation such as the turbulent kinetic energy intensity.

This section will make use of that ability to try to show a relation between the turbulent kinetic energy induced from the twisted plate and corrugations and the heat transfer.

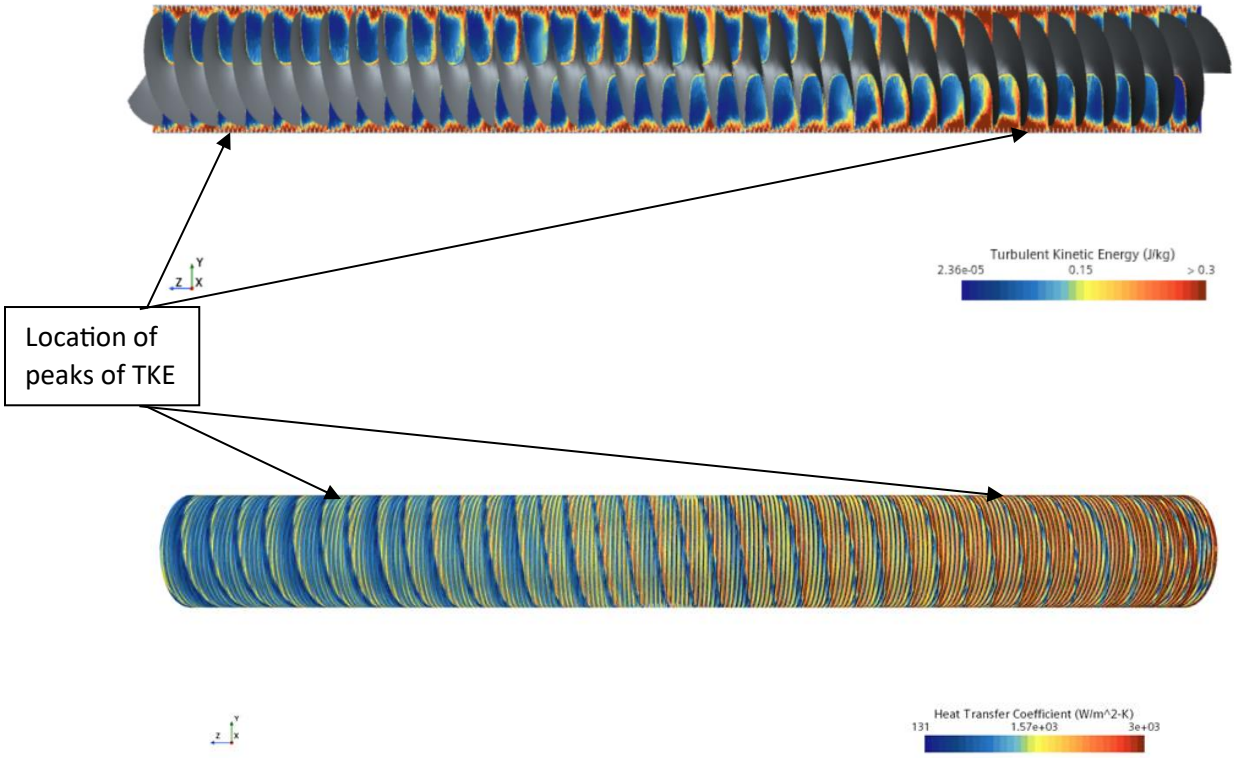

Figure 17 a. Scalar scene for the Turbulent Kinetic energy for tube 5035 b. Scalar scene for the Turbulent Kinetic energy for tube 5035

Figure 17a shows a scalar scene of the turbulent kinetic energy inside tube 5035, an axial plane has been set going through the flow along the tube. It can be noticed that the TKE increases around the twisted tape and near the corrugations.

Figure 17b shows a scalar scene of the heat transfer coefficient across the walls of the tube. It can be noticed that the heat transfer coefficient increases in a similar fashion as the TKE.

4. TUBULAR HEAT EXCHANGER WITH VANES INSERT

The purpose of this section is to introduce a new geometry that will make use of the same enhancement technique which is compound enhancement. The principle behind this is similar to the geometry discussed above as it will induce turbulence inside the tubes using a different insert.

This geometry will attempt to increase the heat transfer at the same level of tube 5035 while trying to keep the pressure drop at a reasonable level to maximize the η factor.

4.1 VANES GEOMETRY DESIGN AND DRAWINGS

The new geometry will be made of 21 Vanes mounted on a 1m long shaft and inserted inside a simple tube of 12 mm diameter with equal spacing between each set of vanes.

Figure 18 Front view of vanes insert.

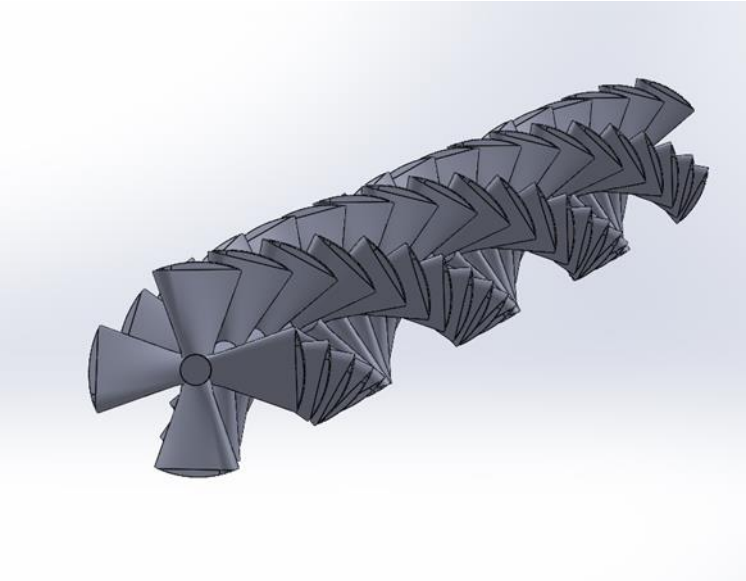

Figure 19 Isometric view of the vane insert.

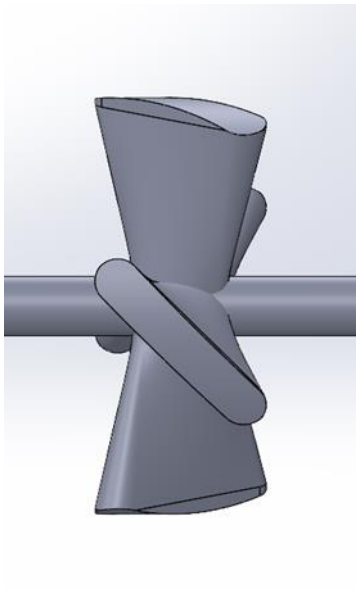

Figure 20 Side view of the vanes.

The geometry was modeled using SolidWorks. The vanes are angled at 135^{o} with respect to the shaft axis. The vanes are equally spaced around the shaft at 45^{o} between each vane. Each vanes set is rotated by 15^{o} from its precedent until eventually completing a full 360^{o} rotation. Four variations were made of this with different spacing between each vane set; 5 cm, 7.5 cm, 10 cm and 12.5 cm.

Figures 21, 22 and 23 show more details about the geometry of the vanes.

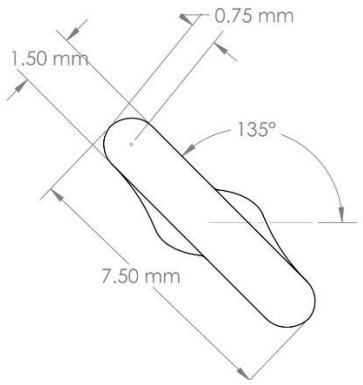

Figure 21 Tip dimensions of the vane.

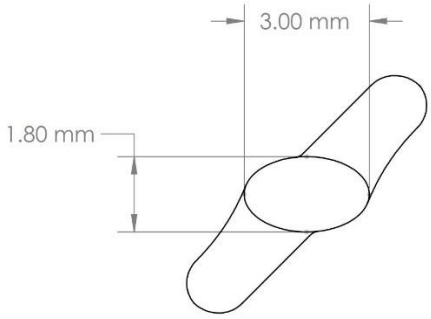

Figure 22 Base dimensions of the vane.

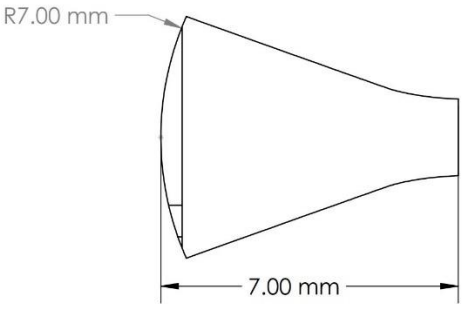

Figure 23 Side dimensions of the vane.

4.2 GRID GENERATION AND PARAMETERS

Since the previous model was validated by the experimental data, the same mesh settings mentioned in section 3.3 will be used for this new geometry.

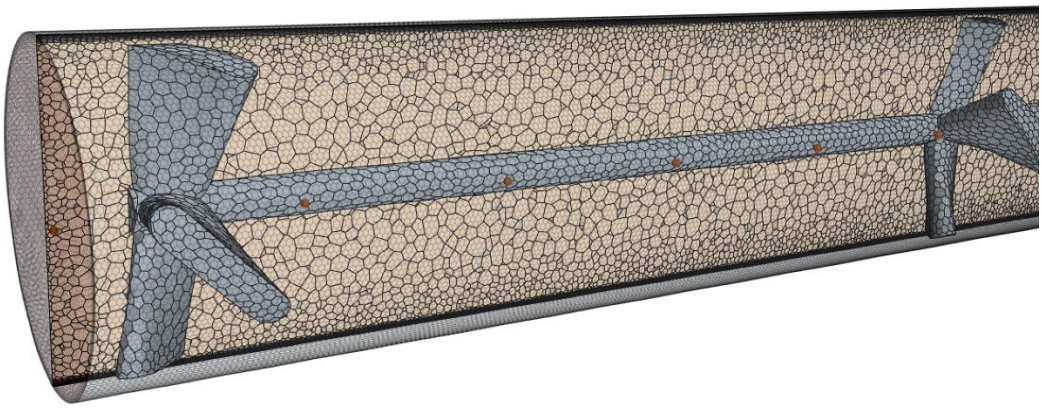

Figure 24 Isometric View of the mesh.

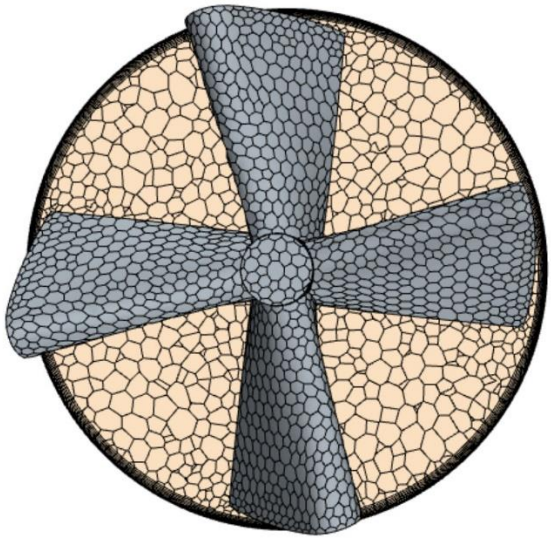

Figure 25 Front view of the mesh.

Figures 24-25 show the construction of mesh after using the same settings as the tube 5035 model. The prism layer can be noticed near the tube wall to capture the temperature gradient, it can be noticed as well that the mesh has an adaptive size; it becomes finer near the walls of the tube and the walls of the vanes to predict turbulence more accurately.

4.3 CFD SIMULATION AND RESULTS

To keep similarity for comparison purposes with the previous model and experimental data, the same boundary conditions presented in section 2.2 are applied for the vane geometry.

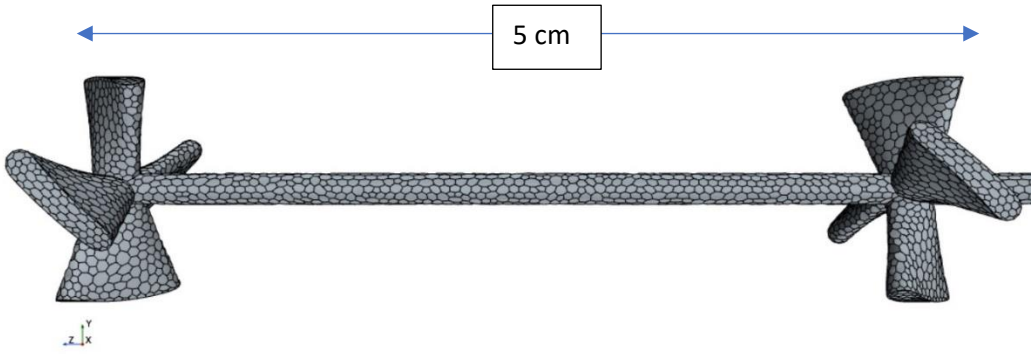

Figure 26 vanes spaced at 5 cm.

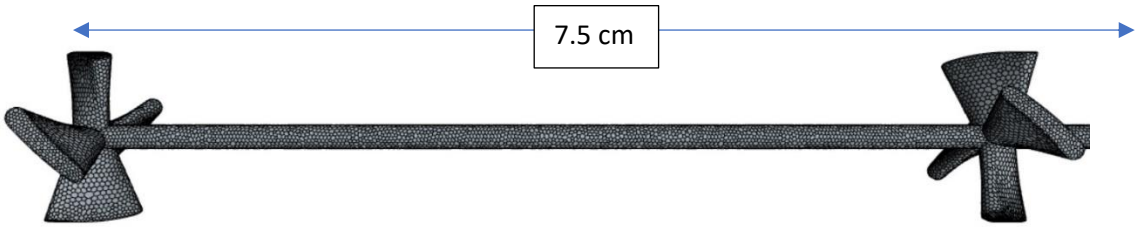

Figure 27 Vanes spaced at 7.5 cm.

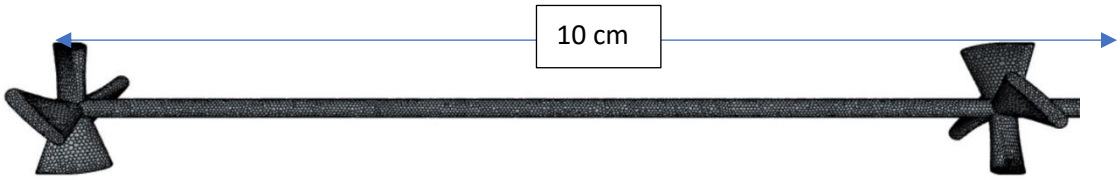

Figure 28 Vanes spaced at 10 cm.

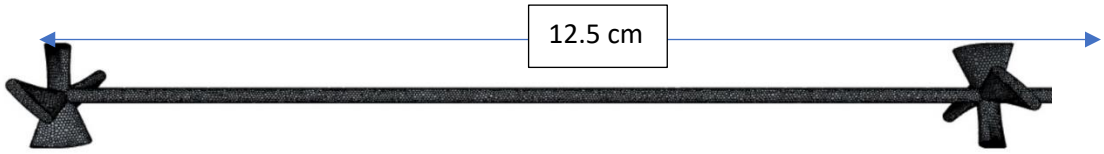

Figure 29 Vanes spaced at 12.5 cm.

Figures 26-29 show the different variations that will be tested in this section.

4.3.1 NUSSELT NUMBER

The Nusselt number was calculated using Eq.1, where h_i is the internal heat transfer coefficient on the inside of the tube in Eq.2. Q is the heat transfer in (W) and was obtained as an output from STAR-CCM+.

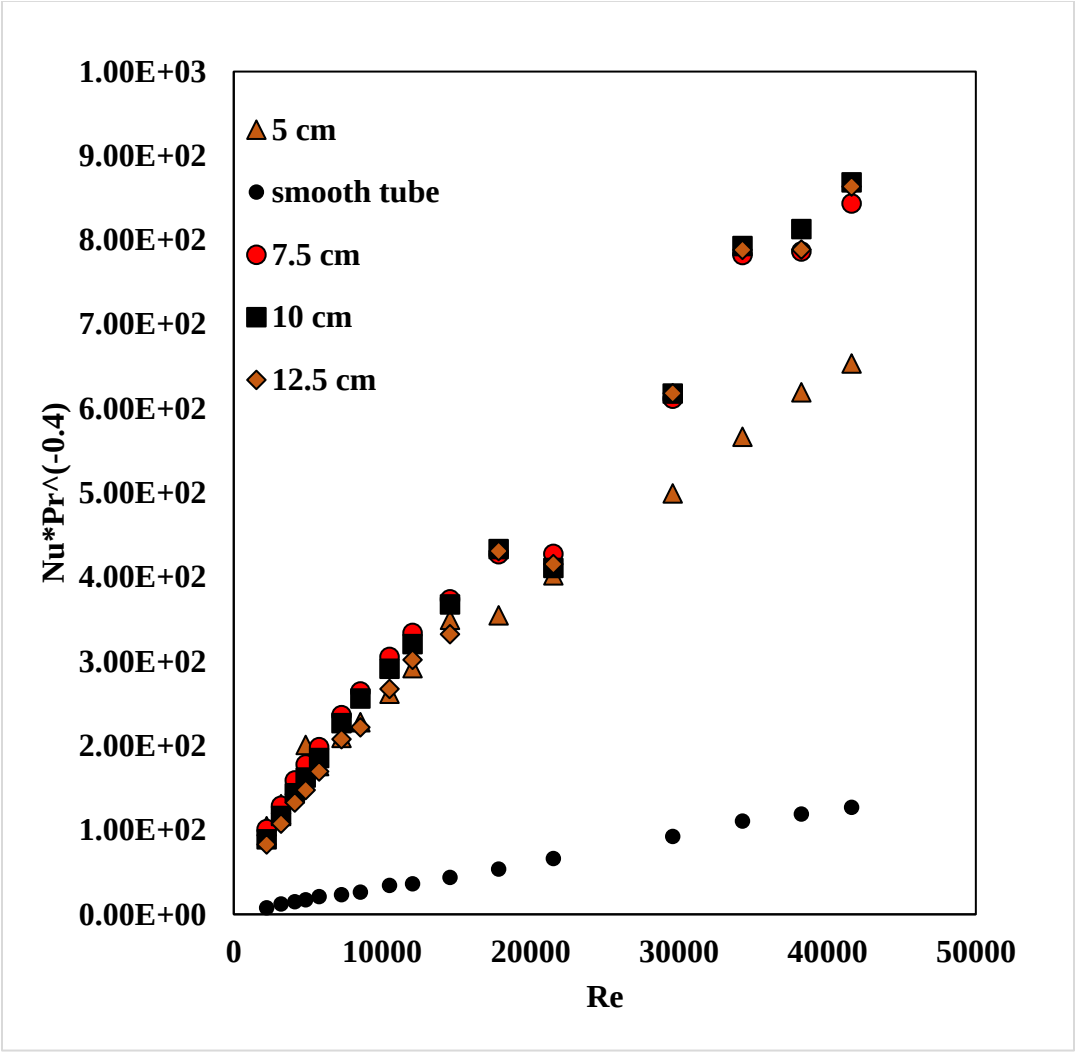

Figure 30 Comparison of the Nusselt number for the vanes variations and smooth tube

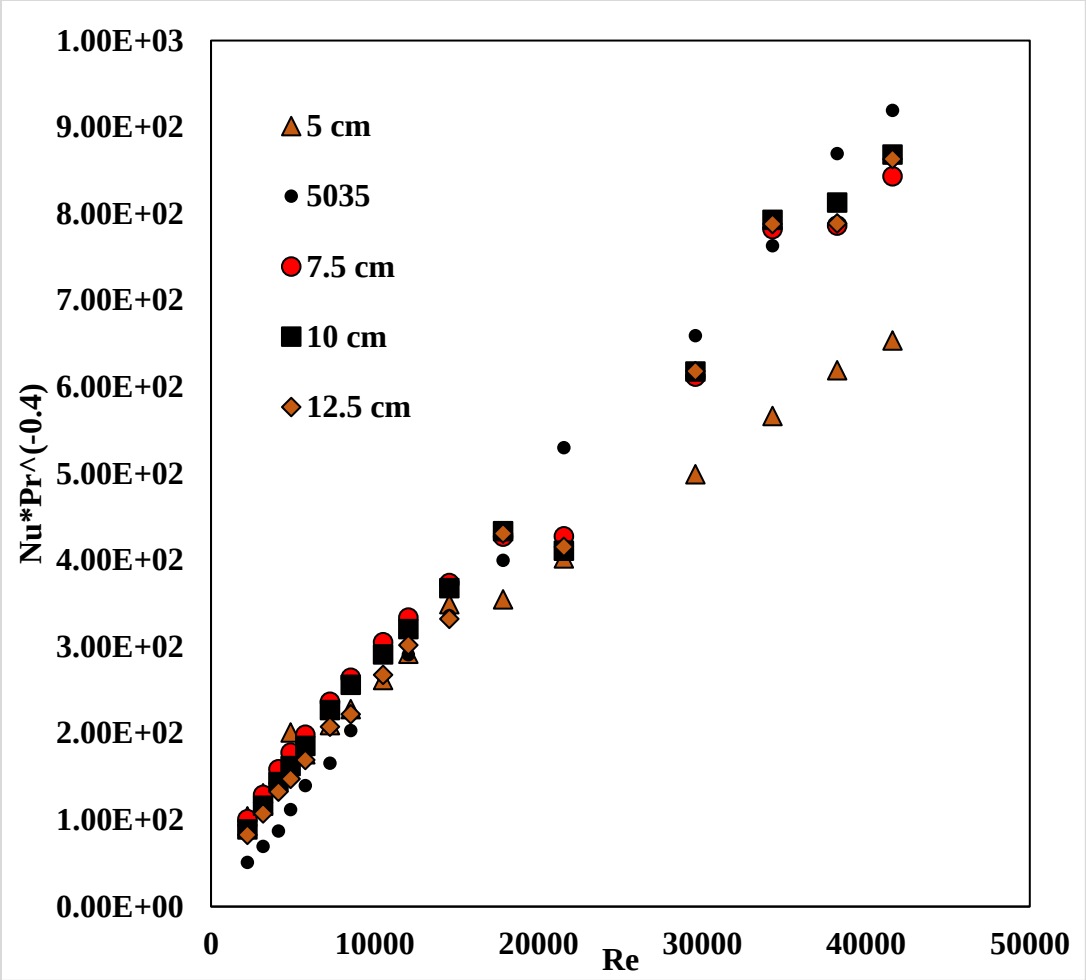

Figure 31 Comparison of the Nusselt number for vanes variations and tube 5035.

From figure 30 it can be noticed that the vanes insert geometry has a Nu. $Pr^{-0.4}$ value considerably higher up to 9 times higher. This was an expected outcome since tube 5035 had the same enhancement. The solid line represent the mean average value.

From figure 31 it can be noticed that the vanes variations had slightly less heat transfer than tube 5035, which was expected since the vanes do not run continuously through the tube, hence the heat transfer through conduction is lesser.

4.3.2 FRICTION FACTOR

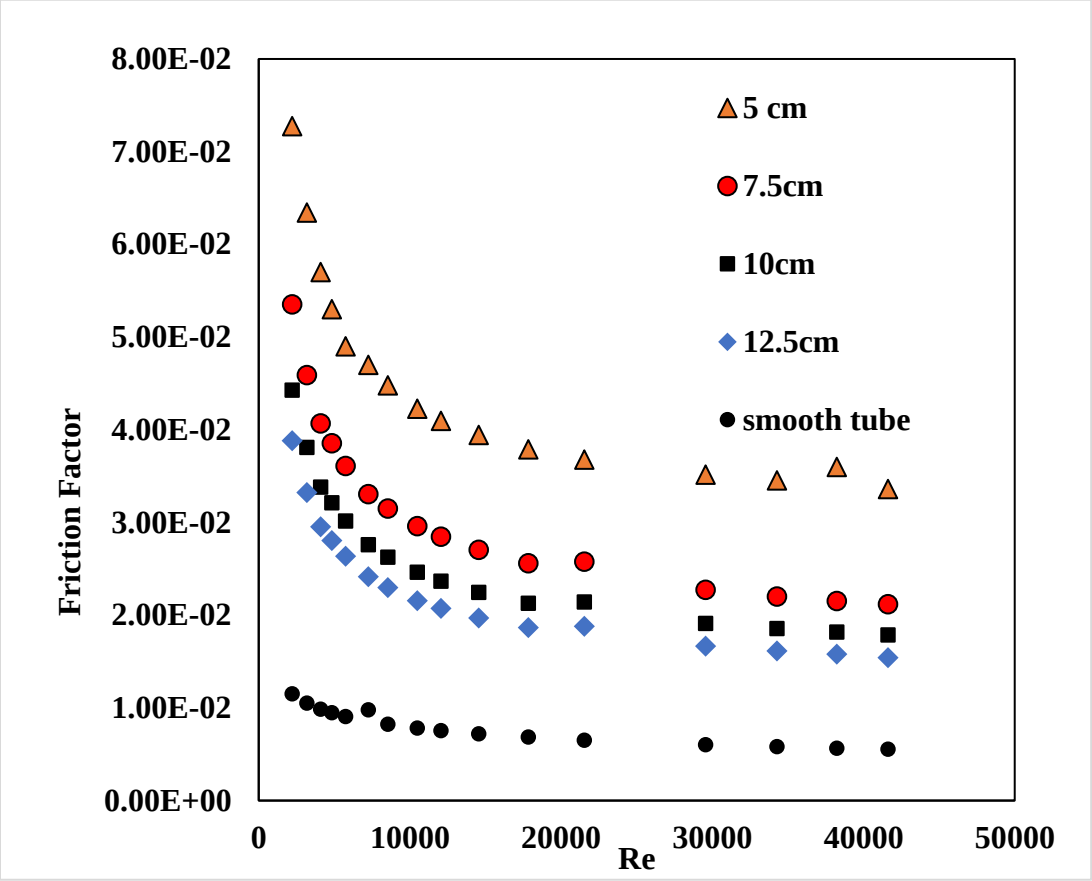

Figure 32 Friction factor comparison of the vanes variations with a smooth tube.

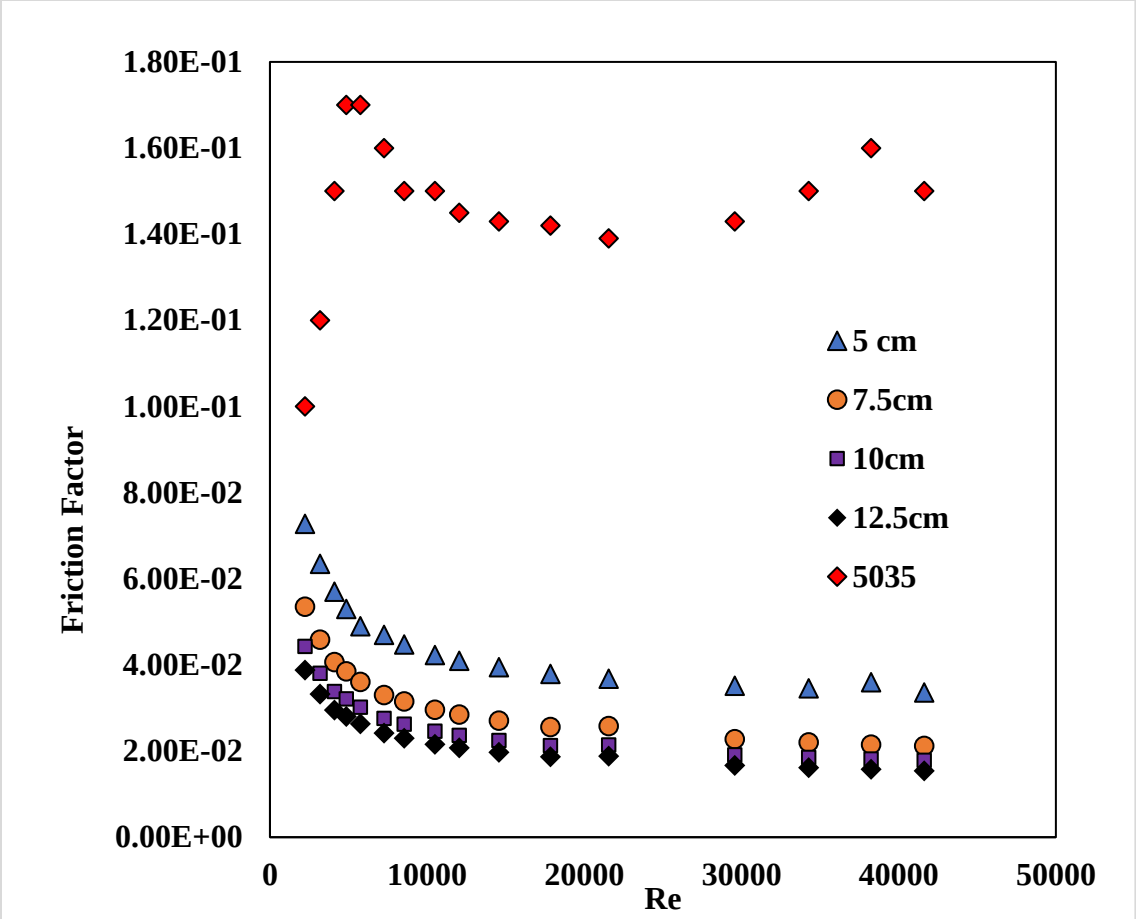

Figure 33 Friction factor comparison of the vanes geometry and tube 5035.

Figure 32 shows that the vanes geometry has a higher friction factor than the smooth tube, which was expected since there is more obstruction to the flow inside the tube, hence causing a higher pressure drop.

On the other hand, the vanes geometry had a considerably lower friction factor value than tube 5035 (figure 33). This was the attempted goal of this

geometry, that by reducing material from the insert there will be less fluid friction and hence less hydro-mechanical losses.

4.4 THERMAL PERFORMANCE

The factor η will allow for a direct comparison between the characteristics mentioned above and the different types of geometries mentioned thus far in this study.

Figure 34 shows η factor calculated for the vanes geometry with the tube 5035 as reference. It can be noticed that the thermal performance ranges from 4 to around 9 for the different variations. The 5 cm spaced vanes had the lowest increase.

The 12.5 cm spaced vane geometry had the biggest enhancement in terms of the η factor. That is mainly due to the significantly lower friction factor shown in figure 33, since the geometries with 7.5-10 and 12.5 cm had roughly the same heat transfer values.

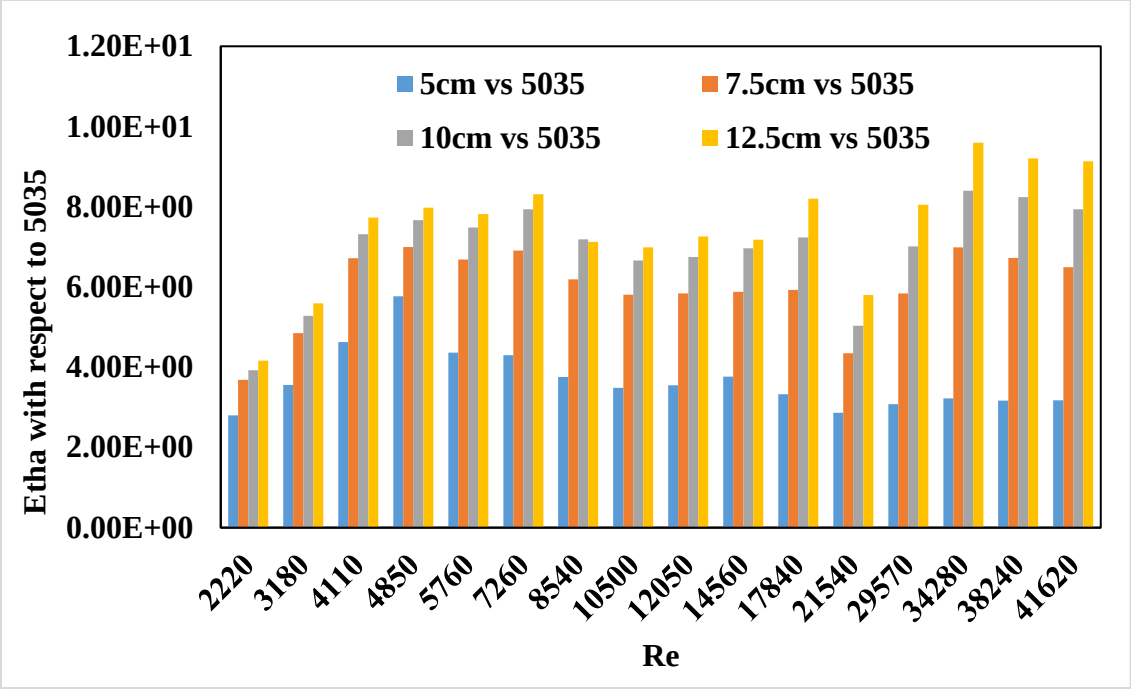

Figure 34 η factor taking the ratios of the vanes geometry and tube 5035.

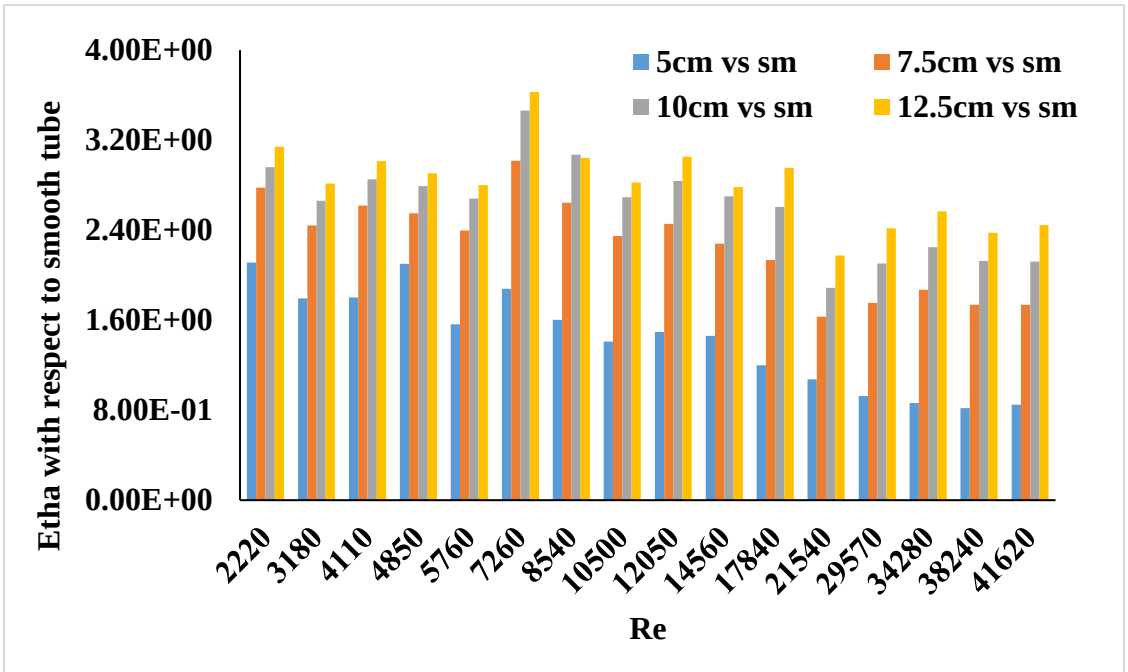

Figure 35 η factor taking the ratios of the vanes geometry and smooth tube.

Figure 35 shows η factor calculated for the vanes geometry with the smooth tube as reference. It can be noticed that the thermal performance ranges from 1 to around 3 for the different variations. The 5 cm spaced vanes had the lowest increase and is the only variation where the η factor is under 1 when Re>25,000.

The 12.5 cm spaced vane geometry had the biggest enhancement in terms of the η factor. That is mainly due to the significantly lower friction factor shown in figure 33, since the geometries with 7.5-10 and 12.5 cm had roughly the same heat transfer values.

Figure 36 Scalar scene showing repeating pattern of increase in turbulent kinetic energy and heat transfer coefficient.

Figure 36 is a scaled down scalar scene for the 12 cm spaced vanes at Re=4400 showing the turbulent kinetic energy inside the flow and its direct effect on the heat transfer coefficient at the walls of the tube.

Figure 37 Streamline view showing swirls created by the vanes.

Figure 37 shows the swirls created by the vanes which are causing the increase in turbulence shown in figure 36. It can also be noticed that the swirls do not diminish in their intensity at 12.5 cm separation between each vane at Re=4400.

To try and investigate more why the 5 cm spaced geometry performed below the rest of the variation at high Re numbers, the CFD software can be used to look more closely at other characteristics such as the turbulent kinetic energy and flow swirls .

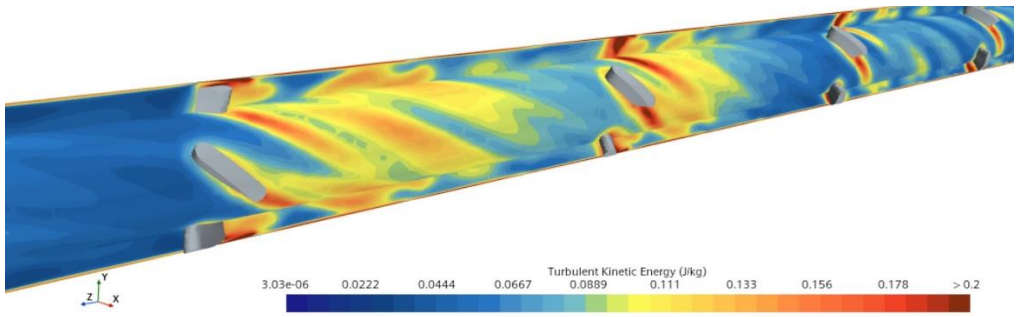

Figure 38 TKE for 5 cm spaced vanes at Re=42,000

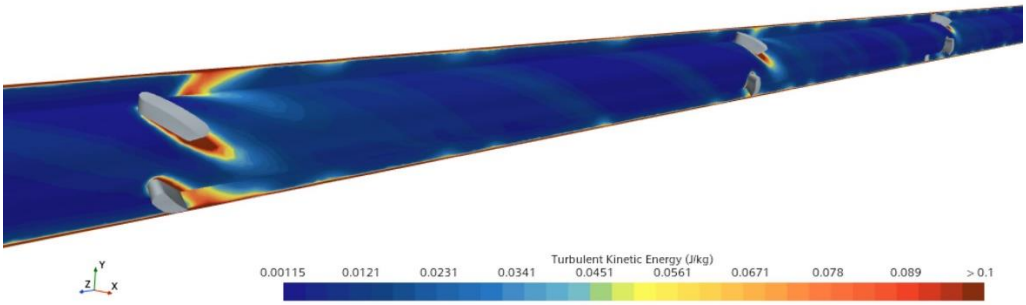

Figure 39 TKE for 12 cm spaced vanes at Re=42,000

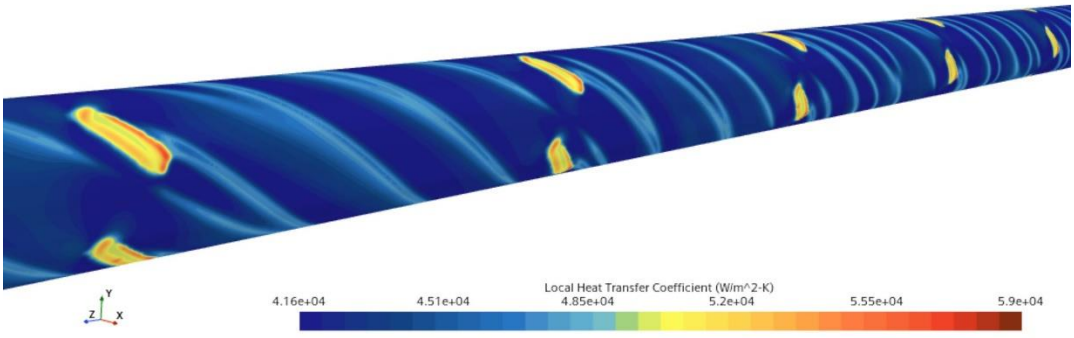

Figure 40 Local Heat Transfer coefficient for 5 cm spaced vanes at Re=42,000

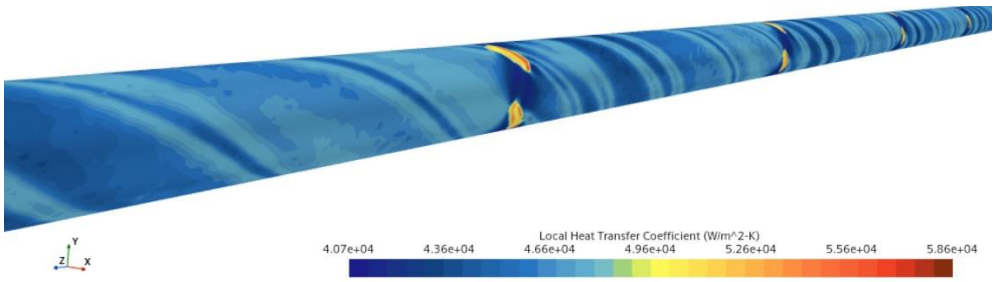

Figure 41 Local Heat Transfer coefficient for 12 cm spaced vanes at Re=42,000

Figures 38 and 39 show the TKE for the 5 cm and 12 cm spaced vanes at Re=42,000 respectively. The 5 cm geometry TKE after the vanes ranges between 0.1 and 0.2 j/kg, considerably higher than the TKE at Re=4,000. While the TKE after the vanes for the 12 cm geometry ranged between 0.03 and 0.001 j/kg.

Similarly figures 40 and 41 show the Local Heat Transfer coefficient. It can be noticed that it decreased for the case of the 5 cm spaced variation where the TKE was much higher compared to the 12 cm spaced ones. The peaks of the Local Heat Transfer coefficient that can be seen on these figures are due to the vanes being in contact with the tube's wall.

Figure 42 Skin friction coefficient for the 5cm geometry.

Figure 43 Skin friction coefficient for the 12 cm geometry.

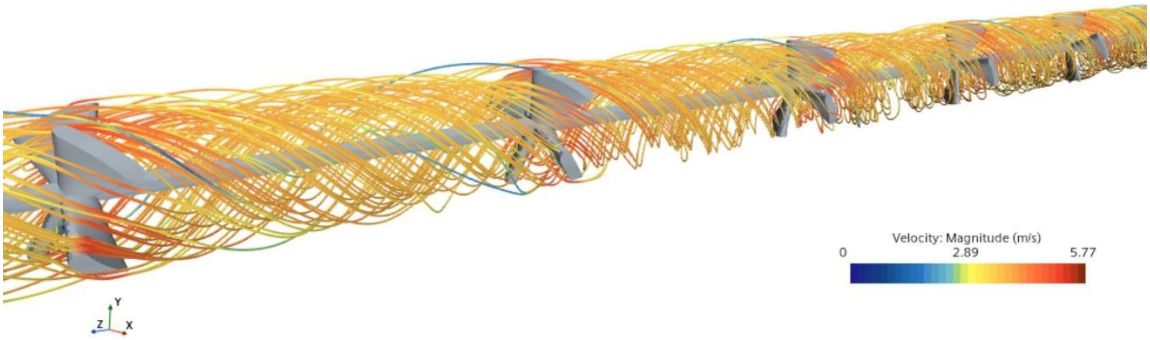

Figure 44 Streamlines showing the velocity magnitude of the 5cm geometry.

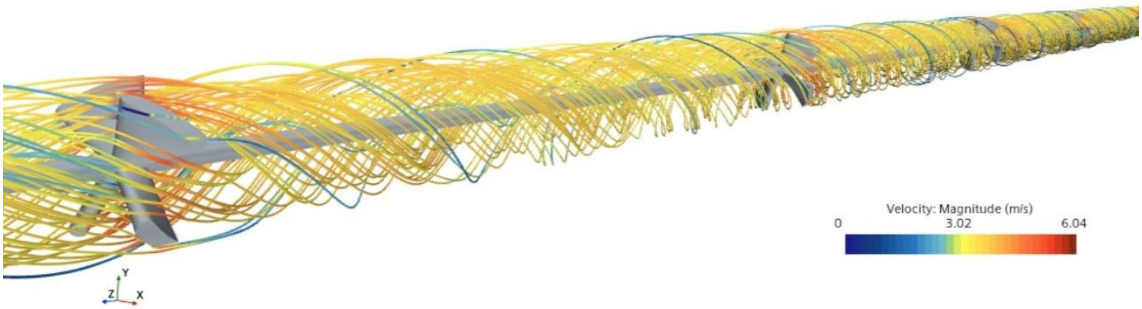

Figure 45 Streamlines showing the velocity magnitude of the 12 cm geometry.

Moving on to the hydrodynamic characteristics, figures 42 and 43 shows the skin friction coefficient for the 5cm and 12 cm geometries respectively. The skin friction coefficient for the 5 cm spaced vanes is slightly higher than the 12 cm spaced vanes. This can be explained by the increased turbulence seen in figure 39 dure to the vanes being closer.

Similarly figures 44 and 45 are showing the velocity magnitude in the streamlines of the flow. The velocity in the 5 cm spaced vanes is lower than the 12 cm due to the same reasons mentioned above. This additional information puts the light on the lower performance exhibited by the 5 cm spaced vanes and makes the 12 cm spacing a much better choice as far as this study is concerned.

CONCLUSION

The enhancement in heat transfer is undeniable in tubes with a twisted insert, but according to this study's CFD results, when the friction caused by the twisted plate is considered, the enhancement is optimal only for Re ranging from 10,000 to 28,000, where 39.6C< T_i <51.5C and 49.3C<T_w<91.8C, where $\eta>1$. For higher Re, the Nusselt number increased significantly due to the elevated turbulence, and thus, an increased mixing of the flow in the transverse direction but with higher friction requires more power to pump the flow, where $\eta<1$.

The CFD model accurately predicted the experimental data, and the parameters used in the model are appropriate and can be replicated in similar simulations.

Figures 11 and 12 show that the compound enhancement method has an undeniable positive effect on the heat transfer coefficient. Tube 5035 with both corrugations and the twisted insert had a heat transfer coefficient 2 to 3 times higher than tube 5030 with only corrugations at the same Re number range. A practical use of such heat exchangers can be in nuclear reactor cooling, automotive radiators, and other applications where tubular heat exchangers are used.

On the other hand, the pressure drop increased significantly as well. Figures 13 and 14 show that tube 5035 experienced more than 2 times the pressure drop when compared to tube 5030 at the same Re number range.

In this study, a new tubular heat exchanger geometry with vanes insert was proposed to enhance heat transfer while maintaining a reasonable pressure drop. The vanes were designed and modeled using SolidWorks, with 21 vanes mounted on a 1m long shaft and inserted inside a 12 mm diameter tube.

CFD simulations were conducted to evaluate the thermal and hydrodynamic performance of the vanes geometry. The Nusselt number was used to assess heat transfer, and it was found that the vanes insert achieved significantly higher Nusselt numbers compared to a smooth tube, up to 9 times higher. However, the heat transfer of the vanes geometry was slightly lower than a tube with continuous enhancement, such as the previously studied tube 5035.

Regarding the friction factor, the vanes geometry exhibited higher values compared to a smooth tube, as expected due to increased flow obstruction. However, the friction factor of the vanes geometry was considerably lower than the tube with continuous enhancement, indicating reduced hydro-mechanical losses.

The thermal performance, evaluated using the η factor, showed that the vanes geometry achieved enhancement ratios ranging from 1 to around 3 for different variations. The 12.5 cm spaced vane geometry demonstrated the highest η factor due to significantly lower friction factors which makes it the better option in this study.

CFD visualizations revealed that the vanes induced turbulence and swirls in the flow, leading to enhanced heat transfer. The intensity of swirls and turbulent kinetic energy remained consistent even at a separation distance of 12.5 cm between the vanes.

Further analysis of the 5 cm spaced vanes at high Reynolds numbers showed higher turbulent kinetic energy, lower heat transfer coefficient, and increased skin friction coefficient compared to the 12 cm spaced vanes. This indicated that the closer spacing of the vanes resulted in higher turbulence but lower overall performance.

Based on the findings of our study, it can be reasonably concluded that the implementation of vanes inserts in the tubular heat exchanger demonstrates promise and effectiveness in enhancing heat transfer performance. These results suggest a potential avenue for further exploration and application in heat

exchanger design and optimization. The 12 cm spacing between vanes appears to be a more favorable choice for achieving a balance between heat transfer enhancement and pressure drop. Further investigations and optimizations can be performed to refine the design and maximize the thermal performance of the vanes geometry.

Overall, this study provides valuable insights into the potential of using vanes inserts in tubular heat exchangers and lays the foundation for further research and development in this area.

REFERENCES

[1] S. Pirbastami, S.F. Moujaes, S.G. Mol Computational fluid dynamics simulation of heat enhancement in internally helical grooved tubes Int. Commun. Heat Mass Transf., 73 (2016), pp. 25-32,

[2] Zimparov, Ventsislav & Petkov, Valentin & Bergles, Arthur. (2012). Performance characteristics of deep corrugated tubes with twisted-tape inserts. Journal of Enhanced Heat Transfer. 19. 1-11. 10.1615/JEnhHeatTransf.2011002711.

[3] P.G. Vicente, A. Garcıa Viedma, A. Experimental investigation on heat transfer and frictional characteristics of spirally corrugated tubes in turbulent flow at different Prandtl numbers Int. J. Heat Mass Transf., 47 (4) (2004), pp. 671-681

[4] E.M. Sparrow, A.T. PrataNumerical solutions for laminar flow and heat transfer in a periodically converging-diverging tube, with experimental confirmation Numerical Heat Transfer, 6 (4) (1983), pp. 441-461

[5] Peng Yang, Hongwei Zhang, Yongyu Zheng, Zhenjian Fang, Xueli Shi, Yingwen Liu, Investigation and optimization of heat transfer performance of a spirally corrugated tube using the Taguchi method,International Communications in Heat and Mass Transfer,Volume 127,2021,105577, ISSN 0735-1933,

[6] Sosnowski, Marcin; Krzywanski, Jaroslaw; Grabowska, Karolina; Gnatowska, Renata. Polyhedral meshing in numerical analysis of conjugate heat transfer EPJ Web of Conferences; Les Ulis, Vol. 180, (2018).

[7] L.M. Jiji, Heat Convection, second ed. Springer, Germany, 2006 22–45

[8] STAR-CCM+ user manual, version 9.04.009. CD-Adapco, 2013.

[9] O. Zikanov, Essential Computational Fluid Dynamics, first ed. Wiley, New York, 2010

[10] K. Ceylan, G. Kelbaliyev, The roughness effects on friction and heat transfer in the fully developed turbulent flow in pipes, Appl. Therm. Eng. 23 (2003) 557–570.

[11]Rahimi, M., Shabanian, S.R., Alsairafi, A.A., 2009. Experimental and CFD studies on heat transfer and friction factor characteristics of a tube equipped with modified twisted tape inserts. Chem. Eng. Process. Process Intensif. 48, 762–770. https://doi.org/10.1016/j.cep.2008.09.007

[12] Gu, H., Chen, Y., Wu, J., Sunden, B., 2020b. Performance investigation on twisted elliptical tube heat exchangers with coupling-vortex square tube layout. Int. J. Heat Mass Transf. 151, 119473. https://doi.org/10.1016/j.ijheatmasstransfer.2020.119473

[13] Gu, H., Chen, Y., Sundén, B., Wu, J., Song, N., Su, J., 2020a. Influence of alternating V-rows tube layout on thermal-hydraulic characteristics of twisted elliptical tube heat exchangers. Int. J. Heat Mass Transf. 159, 120070. https://doi.org/10.1016/j.ijheatmasstransfer.2020.120070

[14]Li, X., Wang, L., Feng, R., Wang, Z., Liu, S., Zhu, D., 2021. Study on shell side heat transport enhancement of double tube heat exchangers by twisted oval tubes. Int. Commun. Heat Mass Transf. 124, 105273. https://doi.org/10.1016/j.icheatmasstransfer.2021.105273

[15]Pirbastami, S., Moujaes, S., 2016. Effect of Groove Dimension on Thermal Performance of Turbulent Fluid Flow in Internally Grooved Tube. https://doi.org/10.1115/IMECE2016-66236

[16]Shaver, D.R., Carasik, L.B., Merzari, E., Salpeter, N., Blandford, E., 2019. Calculation of Friction Factors and Nusselt Numbers for Twisted Elliptical Tube Heat Exchangers Using Nek5000. J. Fluids Eng. Trans. ASME. https://doi.org/10.1115/1.4042889

[17]Su, J., Chen, Y., Wu, J., Fei, F., Yang, S., Gu, H., 2022. Experimental investigation on heat transfer performances in half-cylindrical shell space of different heat exchangers. Int. J. Heat Mass Transf. 189, 122684. https://doi.org/10.1016/j.ijheatmasstransfer.2022.122684

[18]Vahidifar, S., Banihashemi, S., 2023. Experimental and numerical evaluation of heat transfer enhancement by internal flow excitation. Int. J. Therm. Sci. 192, 108395. https://doi.org/10.1016/j.ijthermalsci.2023.108395

[19]Wu, C.-C., Chen, C.-K., Yang, Y.-T., Huang, K.-H., 2018. Numerical simulation of turbulent flow forced convection in a twisted elliptical tube. Int. J. Therm. Sci. 132, 199–208. https://doi.org/10.1016/j.ijthermalsci.2018.05.028

[20]Li, X., Wang, L., Feng, R., Wang, Z., Liu, S., Zhu, D., 2021. Study on shell side heat transport enhancement of double tube heat exchangers by twisted oval tubes. Int. Commun. Heat Mass Transf. 124, 105273. https://doi.org/10.1016/j.icheatmasstransfer.2021.105273

CURRICULUM VITAE

Mouhsine Benmbarek

Email: moebenmbarek@gmail.com

Education

Mississippi State University

MS Mechanical Engineering, 2019

International University of Rabat

BS Aerospace Engineering, 2018

Work Experience

Oldcastle BuildingEnvelope

R&D Engineer, 2023-Present